Experimental Study of Solar Hot Water System Design

Muhannad Sahib Ali

Mech. Eng. Dept.

College of Engineering

Thi-Qar University

Abstract

This paper investigates the design of flat-plate solar collector system experimentally. The production amount of hot water depends on the type and size of the system, the amount of sun rays available at the site, proper installation, and the tilt angle and orientation of the collectors with respect to the south direction. The results show that the amount of the energy collected by the thermal fluid and the absorber plate are inversely proportional to that thickness and diameter of both riser and drum tubes, and it decreases when the air gab between glasses layer increases (prevents the sun rays and the solar effect). The intensity of the mean sun rays daily per hour is an important factor to the energy absorbed by the collector. This study used aluminum as an absorber plate because its thermal conductivity is high more than copper and mild steel, its price is cheap.

دراسة عملية لتصميم منظومة سخان شمسي

المستخلص

في هذا البحث تم دراسة عملية لتصميم سخان شمسي نوع الصفيحة المستوية يستخدم لتسخين المياه. حيث أن كمية الماء الساخن المحصلة من استخدام السخان الشمسي تعتمد على نوع وحجم السخان المستخدم، كمية الإشعاع الشمسي المتوفر في موقع العمل، الربط المناسب زاوية واتجاه المجمعات الشمسية بالنسبة للاتجاه الجنوبي. النتائج أوضحت أن كمية الطاقة الحرارية الممتصة من قبل الصفيحة الماصة والماء الساخن تتناسب عكسياً مع سمك وقطر الأنابيب سواء كانت المجمعة أو الصاعدة ، كما إن الطاقة الممتصة تزداد بزيادة عدد الأغطية الشفافة الزجاجية ألا أنها تقل بزيادة المسافة بين الأغطية الزجاجية لأنها تمنع أو تقلل من تأثير أشعة الشمس. أن شدة معدل الإشعاع اليومي للشمس في الساعة تلعب دوراً أساسيا في كمية الطاقة الممتصة. في هذا البحث تم استخدام الألمنيوم كصفيحة ماصة للحرارة كونه موصل جيد للحرارة كما أن الألمنيوم متوفر في الأسواق المحلية وثمنه ارخص.

1. Introduction

Solar energy is radiant energy that is produced by the sun. Every day the sun radiates, or sends out, an enormous amount of energy. The sun radiates more energy in one second than people have used since the beginning of time.

The sun is a big ball of gases mostly hydrogen and helium atoms. The hydrogen atoms in the sun's core combine to form helium and generate energy in a process called nuclear fusion.

It takes millions of years for the energy in the sun's core to make its way to the solar surface, and then just a little over eight minutes to travel the 93 million miles to earth. The solar energy travels to the earth at a speed of 186,000 miles per second, the speed of light.

Only a small portion of the energy radiated by the sun into space strikes the earth, one part in two billion. About 15 percent of the sun's energy that hits the ear this reflected back into space. Another 30 percent is used to evaporate water, which, lifted into the atmosphere, produces rainfall. Solar energy also is absorbed by plants, the land, and the oceans. The rest could be used to supply our energy needs.

More than 100 years ago, a scientist used heat from a solar collector to make steam to drive a steam engine[1]. In the beginning of this century, scientists and engineers began researching ways to use solar energy in ear nest. One important development was a remark ably efficient solar boiler invented 1936. The public and world governments remained largely indifferent to the possibilities of solar energy until the oil shortages of the 1970.

May be more important for the purposes of collecting solar energy to heat water is that the sun comes to us in three different forms: (1) direct parallel rays; (2) diffuse radiation, which comes to us from all directions after being glanced off clouds, dust or moisture particles in the air; and (3) reflected radiation, which has been bounced straight off some surface[2,3].

Today there are more than 30 million m^2 of solar collectors installed around the globe. Hundreds of thousands of modern solar water heaters, are in use in countries such as China, India, Germany, Japan, Australia and Greece. In fact, in some countries the law actually requires that solar water heaters be installed with any new residential construction project. People use solar energy to heat buildings and water and to generate electricity[4,5].

In spite of the aforementioned work for the hot water solar system, there is a gap in the heat transfer literature for the system design and the equation and factors depends in design. The object of the present study is to fill this gap and provide a basis for the validity of the approximate analysis presented by other researchers [6,7,8]. Further gives the behavior of the temperature of the hot water inside the storage tank with difference in any member of constructions.

2. Governing equations

$$Q_E = Q_L + Q_I \quad (1)$$

$$Q_E = I_h * f * HT * A \quad (2)$$

$$Q_L = U_f * HT * A * \Delta T \quad (3)$$

$$Q_I = \dot{\sigma} * C(t_{f,e} - t_{f,i}) \quad (4)$$

$$t_{f,e} = t_{f,i} + (T_p - t_{f,i})[1 - \exp(-H/\dot{\sigma} * C)] \quad (5)$$

$$C = G_m * C_m + g * C_w \quad (6)$$

$$f = A_f . T_{rf} \quad (7)$$

$$\frac{(t_{f,e} - t_{f,i})}{Q_E} = \frac{1}{\dot{\sigma} * C}\left[1 + \frac{U_c}{\dot{\sigma} * C\left[1 - \exp\left(-\frac{H}{\dot{\sigma} * c}\right)\right]}\right]^{-1}\left[1 - \frac{U_c\,(t_{f,i} - t_a)}{Q_E}\right] \quad (8)$$

$$I_{daily} = S\int_{t1}^{t2} e^{-\tau/\cos z}\cos\theta \, dt \quad (9)$$

$$T_m = t_a + (t_{f,e} - t_a)\exp(-\overline{U}_L * L/\dot{m} * c) \quad (10)$$

$$m_{fuel} = Q_I * HT * 320/H_0 \quad (11)$$

3. System configuration

A schematic diagram of the solar system modeled is shown in Figure (1). Flat solar collector is a very simple. It consists of an insulated rectangular box. It contains a metal plate that has been painted black, with a pipe at each end (called headers) that are connected to small tubes (called risers) also made from pipe. Water is first heated in the risers and then returns to the storage tank. The entire box is covered with a special glass that is hail resistant. The storage tank contains water that accumulates heat obtained from the hot water. The cold water enters the storage tank at the bottom, and the supply hot water exits from the top.

3.1. Flat collectors with glass cover

A flat-plate collector Figure(2) consists of an absorber, a transparent glass cover, a frame, and insulation material. Usually an iron-poor solar safety glass is used as a transparent cover, as it transmits a great amount of the short-wave light spectrum. Simultaneously, only very little of the heat emitted by the absorber escapes the cover (greenhouse effect). In addition, the transparent cover prevents wind and breezes from carrying the collected heat away (convection) and also prevent the accumulation of dirt on top of the absorber surface. The insulation on the back of the absorber and on the side walls lessens the heat loss through conduction, generally frame made from wood with dimensions (1×2)m and height 0.1m, it is covered with aluminum plate to protect it and the aluminum is very good to resist the corrosion.

3.2.The absorber

The heart of a solar collector is the absorber. Absorber was made from aluminum plate (1×2)m and painted black, as dark surfaces demonstrate a particularly high degree of light absorption. As the absorber warms up to a temperature higher than the ambient temperature, it gives off a great part of the accumulated solar energy in form of long-wave heat rays. The ratio of absorbed energy to emitted heat is indicated by the degree of emission. In order to reduce energy loss through heat emission, the most efficient absorbers have a selective surface coating. This coating enables the conversion of a high proportion of the solar radiation into heat, simultaneously reducing the emission of heat. The selective coatings provide a degree of absorption up to 90%.

3.3. Hot water storage tank

The purpose of the hot water storage tank is to stockpile energy for days with less solar radiation. Its volume capacity should be larger than the daily hot water consumption, to avoid a lack of hot water, when there is less sun. Good solar storage tanks have a slim, cylindrical form in order to develop a layering of temperature in the tank. This allows for optimal usage of the heated potable water in the upper storage region, thus the entire contents of the tank don't need to be heated to the desired temperature.

Because heat tends to rise, insulation does the most good above the heat source. Any extra material should be put at the top of the tank. Another way to insulate a tank very well is to build a ply wood box around the tank and fill it with insulation Figure(3).

Insulation fills all the nooks and crannies around the tank, and it's just a matter of mixing two liquids together and pouring them into the box. The mixture will expand, foam and bubble like a witch's brew, and work its way into all the spaces between the tank and the plywood.

4. Results and discussion

A thermo siphon system relies on warm water rising, a phenomenon known as natural convection, to circulate water through the collectors and to the tank. In this type of installation, the tank must be placed above the collector. As water in the collector heats, it becomes lighter and rises naturally into the tank above. Meanwhile, cooler water in the tank flows down pipes to the bottom of the collector, causing circulation throughout the system. The storage tank is attached to the top of the collector so that thermo siphoning can occur.

4.1. Solar energy

There are four factors that affect the amount of heat captured by a flat plate collector: (1) the solar intensity (2) the collector's orientation toward the sun, usually to the south,(3) the temperature of the air surrounding the collector call the ambient air and (4) the materials used in the collector itself, specifically the quality of the glazing and the material selected for the key component, the absorber plate.

Equation {G=(D-t)×k } shows that the effect of the thickness of the pipes (riser, drum) on the heat transfer energy. Figure(4) shows that any increasing in the thickness causes decreasing in the temperature of hot water in storage tank because the bigger thermal resistance and much time to the same temperature.

The continuity equation and Figure(5 and 6) show that the opposite relation between the heat energy and diameter to both riser and drum pipes, when the diameter increase the area and the flow rate is greater due to that no enough time to heated fluid pass through pipes so the absorbed energy relative to the mass flow rate.

The important job of the glass cover is to reduce the energy losses and allow to the sun rays absorbed by the dark plate. We must decrease thickness of the glass cover to increase the permeability and due to that absorbed energy increasing Figure(7).

This paper studies the effect of the glasses cover number, glass heat transfer coefficient increase when the gap between glasses layer decrease and Figure(8) shows that when glasses heat transfer coefficient increasing the temperature decrease because the gap between glasses

layer prevent the sun rays deflected to the atmosphere and reduce the energy losses by conduction and convection, the effect of two glasses layer more better than one glass cover.

Figure(9) shows that any increase in the mean daily average of the sun rays cause increase in the heat energy.

In this paper examined many metal (aluminum, copper and mild steel) to made black plate, from Figure(10) shows that the aluminum is the best metal to absorbed energy and any increasing in metal thickness decrease in temperature because the plate must be in a thermal balance then the heat transfer from it to the pipes and this is need more time.

The experimental result for the temperature is shown in Table (1); the absorbed amount of the sun rays is higher with the angle of the solar collector orientation is equal to 45 degree and to the south.

Table (1). Measured temperature .

$T_{dark\ plate}$	$T_{out\ of\ collector}$	$T_{inside\ collector}$	Orientation
76°C	58°C	22°C	
81°C	65°C	21°C	
82°C	71°C	23°C	45°
80°C	69°C	25°C	
51°C	46°C	25°C	
55°C	47°C	24°C	
78°C	58°C	24°C	30°
77°C	48°C	23°C	
77°C	59°C	23°C	

4.2. Economic benefits

This paper analysis illustrates that the initial installed cost of the solar water heater ($700), it is higher than that of a gas water heater ($350 to $450) or an electric water heater ($150 to $350). The costs vary from region to region. Depending on the price of fuel sources, the solar water heater can be more economical over the lifetime of the system than heating water with electricity, fuel oil, propane, or even natural gas because the fuel (sunshine) is free. To determine the simple payback of a solar water heater by determining the net cost of the system then calculate the annual fuel savings and divide the net investment by this number to determine the simple payback. This study expected a simple payback of 4 years.

5. Validation of the results

In order to check the validity of the present study, a comparison is made with a Delfin Sili Salcines. A comparison of the heat energy calculation with the experimental data table 2 shown it seam that, the result have good agreement and the average error is (1%).

Table (2)

Experimental heat energy	Delfin Sili Salcines
366.976	364.886
352.585	350.225
330.998	328.564

6. Conclusions

Passive systems move household water or a heat-transfer fluid through the system without pumps. Passive systems have no electric components to break. This makes them generally more reliable, easier to maintain, and possibly longer ages and economical.

1. To maximize the amount of solar energy collected in a passive solar system you can increase the size of the solar collector, and ensure that the position of the tank and system get optimum sunlight.
2. Concentrates the sun’s rays on the collector (glass cover number), which maximizes the heat energy transferred to the water.
3. Use black absorbs light because it has no color to reflect.
4. Use materials (Aluminum) to further focus the sun’s energy; insulate the collecting tank, check the sun’s angle at different times of the year; use a thermal mass under and around the collector etc.
5. Some limitations are hot water storage at night, when the sun is not available (good insulation would be required).
6. Sunlight has no cost; oil supplies will not be depleted so fast, if solar energy is part of our energy mix; energy bills would be less; less pollution would be emitted.

Figure (1). A thermo siphon solar water heater uses a free-circulating panel.

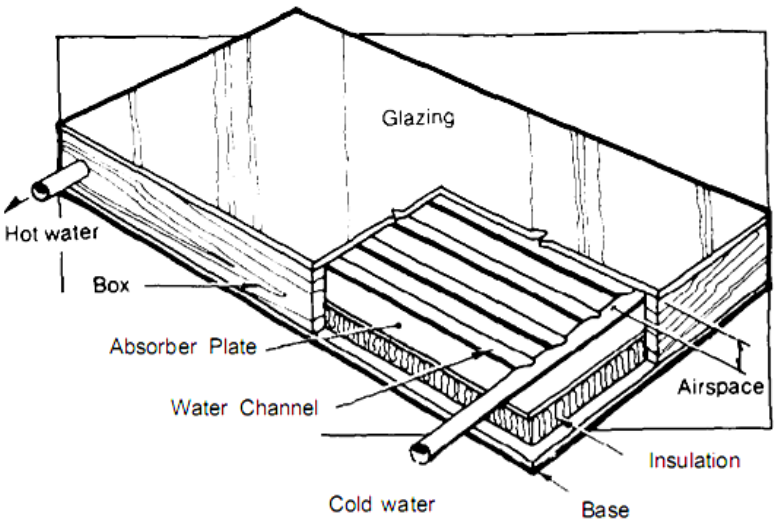

Figure (2). Flat plate solar collector.

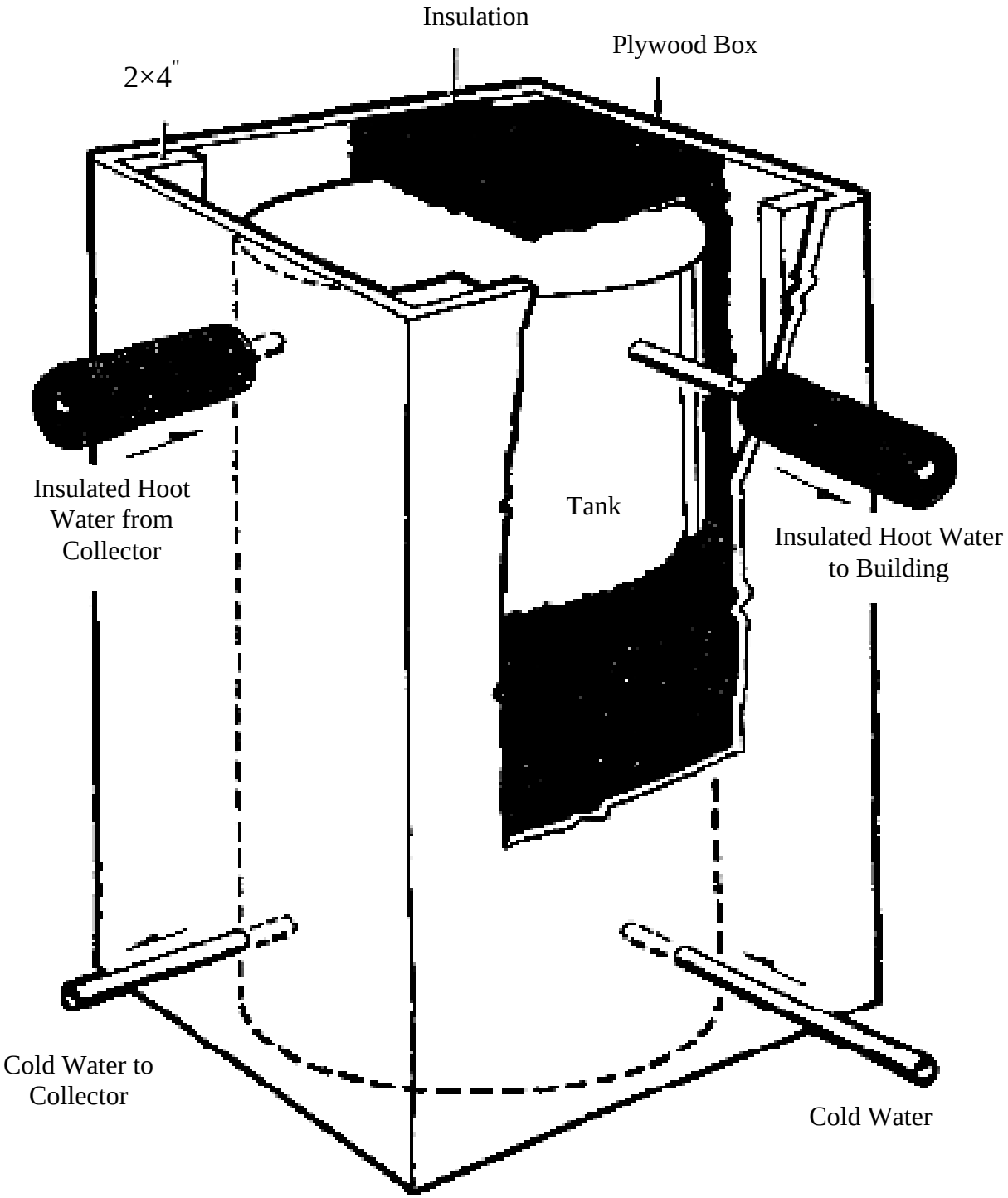

Figure (3) .Solar hot water tank.

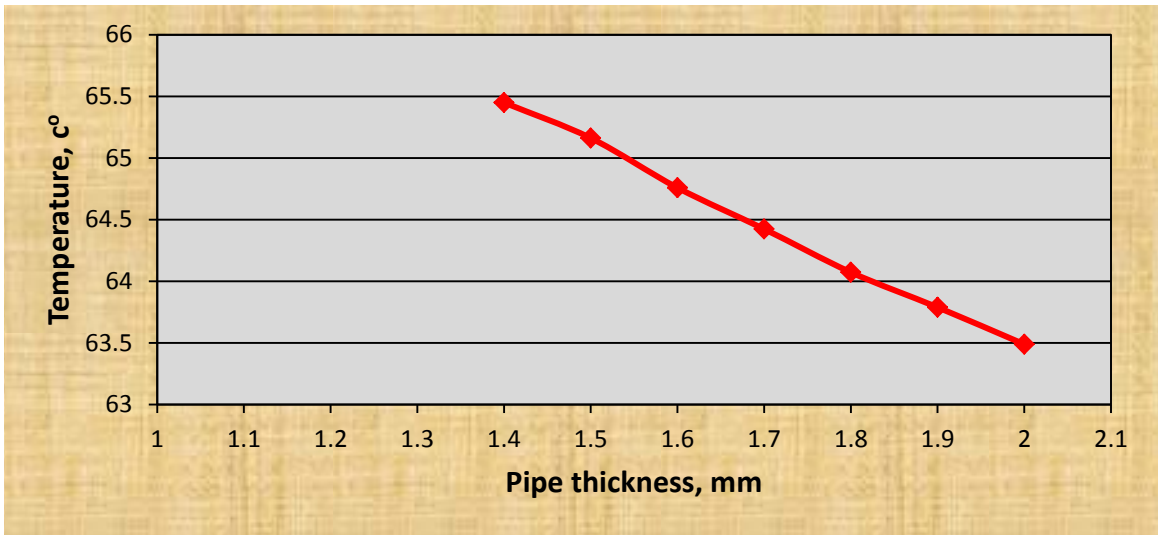

Figure (4). Pipe thickness effect.

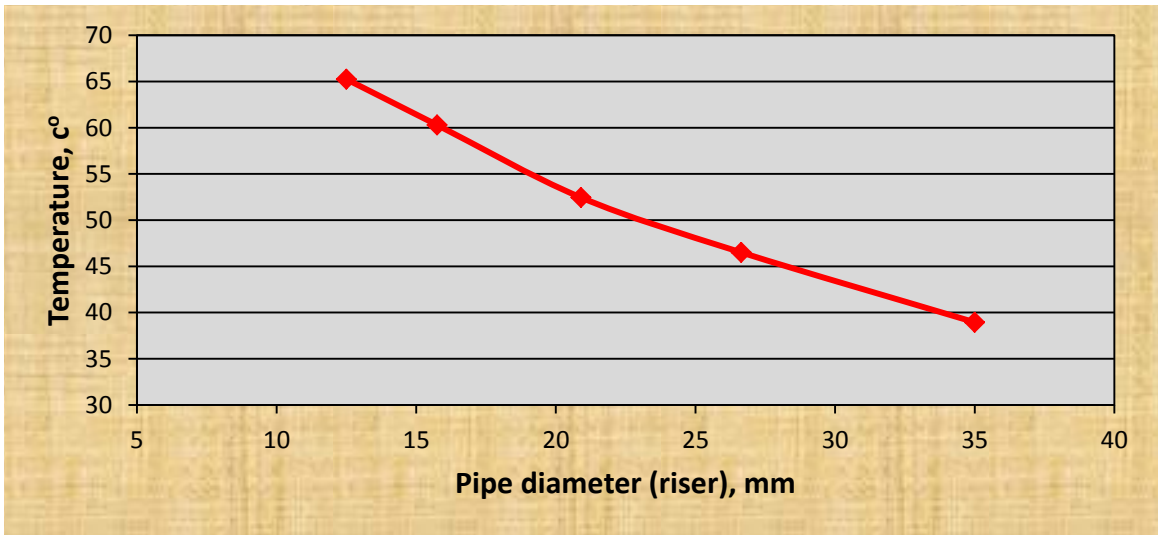

Figure (5). Pipe diameter (riser) effect.

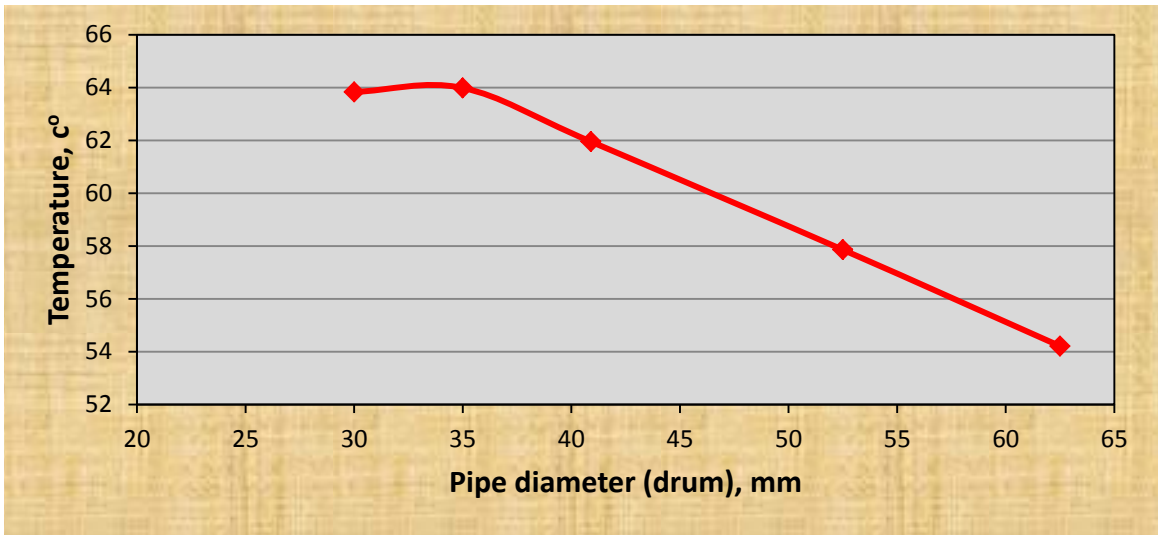

Figure (6). Pipe diameter (drum) effect .

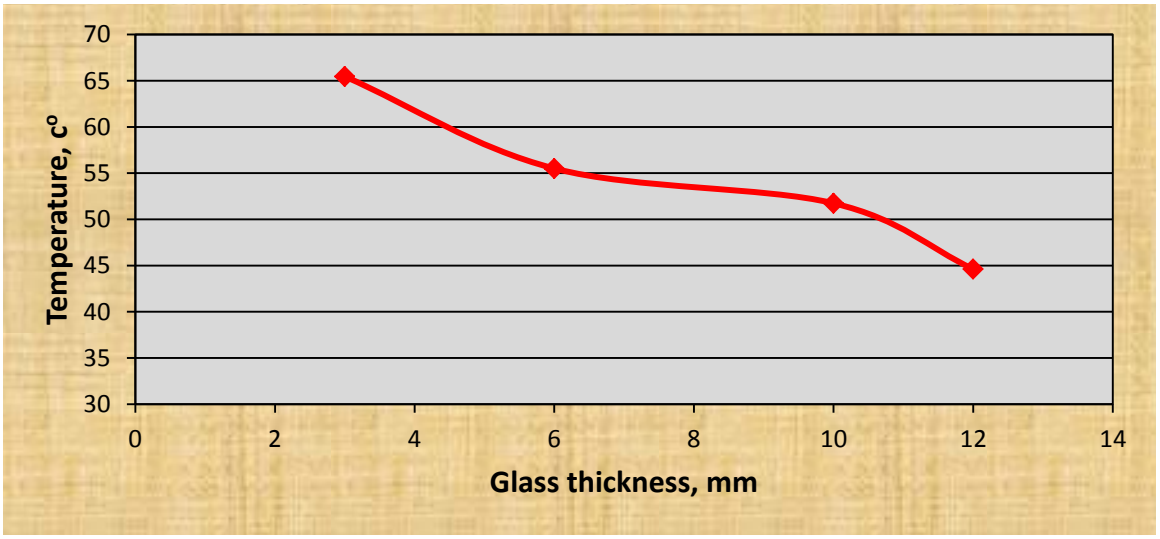

Figure (7). Glass thickness effect.

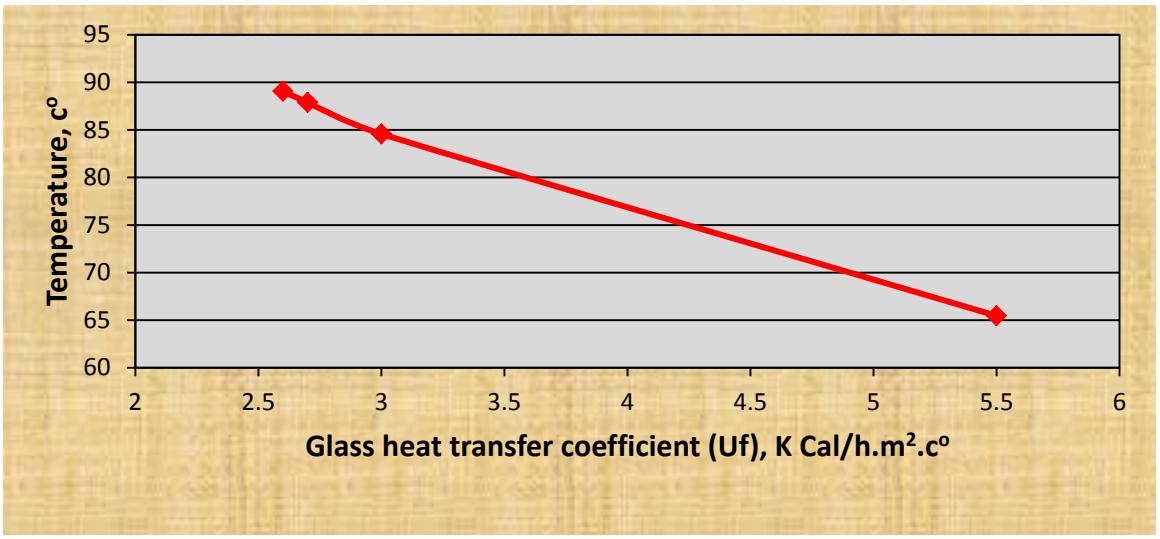

Figure (8). Glasses number effect.

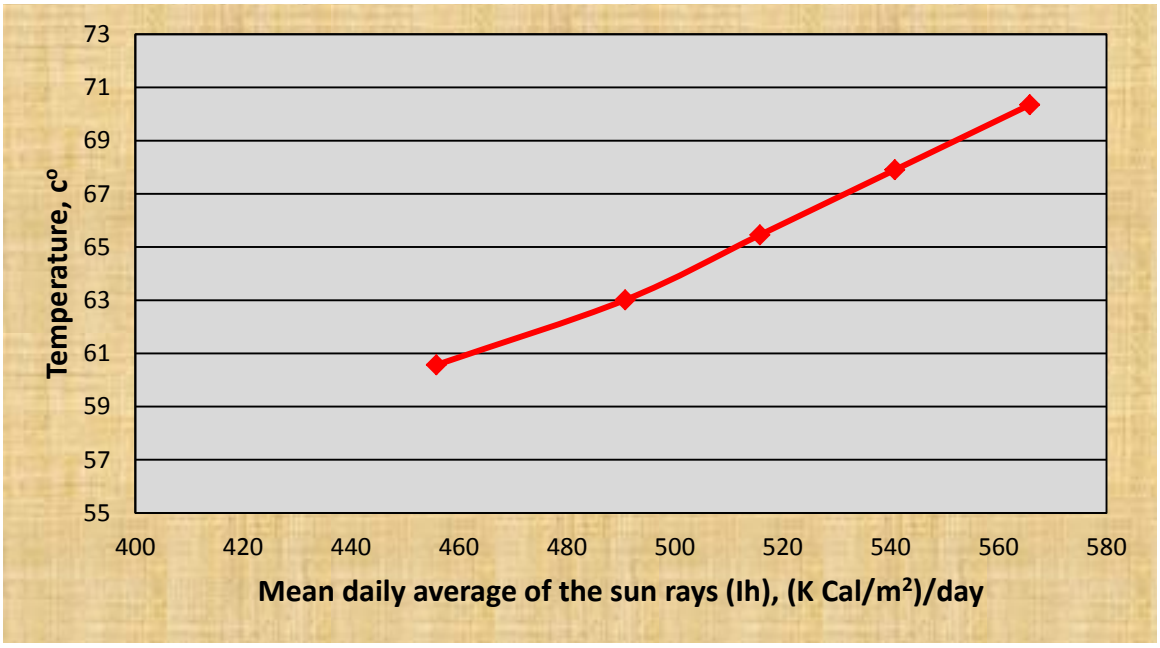

Figure (9). Mean daily average of the sun rays effect.

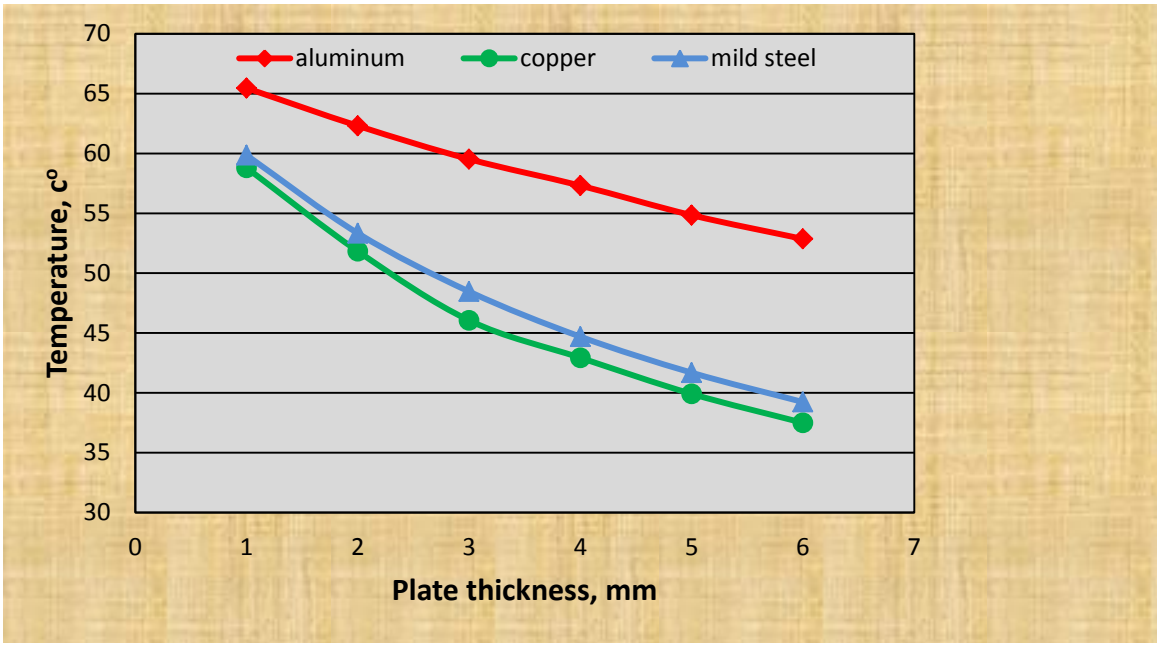

Figure (10). Plate thickness effect.

7. References

[1]د. سعود يوسف عياش، " تكنولوجيا الطاقة البديلة"،المجلس الوطني للثقافة والفنون،1980 .

[2] د. أمين القلق ، " سلسلة الحقائق التعليمية التدريبية في مجال الطاقات المتعددة " ، المركز الوطني لبحوث الطاقة .

[3] سول وايدر ، " مقدمة في الطاقة الشمسية"، مديرية دار الكتب للطباعه والنشر جامعة الموصل، 1989-1991.

[4] م. مظفر سمير عميش ، " السخانات الشمسية وطرق توصيلها بشبكة المياه الساخنة للأنظمة الهامدة والقسرية " المركز الوطني لبحوث الطاقة، 1993 .

[5]Minister of Natural Resources Canada 2001 – 2004"Solar water heating project analysis chapter" ISBN: 0-622-35674-8

[6] Stu Campbell with Douglas Taff, Ph.D. "Build your own solar water heater" Library of Congress Cataloging in Publication Data Campbell, 1942

[7] Delfin Silió Salcines, Carlos Renedo Estébanez and Valentin Castaöera Herrero "Simulation of a solar domestic water heating system, with different collector efficiencies and different volume storage tank" Department of Electrical Engineering, E.T.S.I.I. yT., Cantabria University.

[8] Duffie JA, Beckman WA. Solar engineering of thermal processes. 2nd ed. New York: Wiley, 1991.

8. Nomenclature

$\overline{U}_L$= losses longitudinal heat transfer coefficient

A_f=absorption glass coefficient

m_{fuel}= The annual fuel savings

T_p= plate temperature

T_{rf}= permeability glass coefficient

U_c= losses heat transfer coefficient

$\dot{\sigma}$ = average flow rate

A = solar collector area

Af= glass absorber coefficient

C = solar collector thermal capacity

D = pipe diameter

g_m = capacity of the pipe metal mass

Gm = weight of the metal mass for absorber plate and pipe

H = heat transfer coefficient

H_o= oil thermal capacity

HT = the daily average of the sun rays time

Iday = the daily average of the sun rays

L= pipe length

QE = solar energy per hour land on the solar collector

QI = solar energy per hour absorbed by the solar collector

QL = solar energy per hour losses by the solar collector

t = thickness

T= temperature

Tf = glass permeability coefficient

$t_{f,e}$ = hot water temperature

$t_{f,i}$ = cold water temperature

t_a= ambient temperature

Tm = hot water temperature in storage tank

U_f = glass heat transfer coefficient

θ= acceptance angle

ρ= density

Analysis of Solar Powered Air Conditioning Systems for Residential Applications

Mushtaq Ismael Hasan
Mech. Eng. Dept.
College of Engineering
Thi-Qar University
mushtaq76h@yahoo.com

Mohammed D. Salman
Mech. Eng. Dept.
College of Engineering
Thi-Qar University

Ghassan Adnan Abid
Mech. Eng. Dept.
College of Engineering
Thi-Qar University

Abstract

In this paper the absorption air conditioning system has been analyzed, and the solar energy has been used as a source for heat required to operating the absorption cycle. The influence of most of the parameters which may affect the performance of absorption air conditioning system has been studied under the climatic conditions of Iraq. The main advantage of solar based air conditioning systems is the synchronization between the cooling demand and the availability of solar energy especially in hot regions like Iraq which contains huge potential of solar energy in summer season. The results obtained indicate the ability of using solar energy to reduce the electricity consumption for air conditioning applications. For a certain space with cooling load 5 Ton (17.5 kW) for climatic conditions (solar radiation intensity 1000 W/m^2 and ambient temperature 45 ^{o}C) the solar collector with area 40 m^2 can provide 75% of required heat to produce this cooling load demand and a collector with area 53 m^2 can provide 100 % of required heat to produce this cooling load demand for these climatic conditions.

تحليل منظومات التكييف التي تعمل بالطاقة الشمسية للتطبيقات المنزلية

المستخلص

في هذا البحث تم دراسة وتحليل منظومة تكييف الهواء الامتصاصية وتم استخدام الطاقة الشمسية كمصدر للحرارة اللازمة لتشغيل هذه الدورة الامتصاصية. تم دراسة تأثير معظم العوامل التي من الممكن أن توثر على أداء منظومة تكييف الهواء الامتصاصية بالظروف المناخية للعراق.

الميزة الأساسية لمنظومات التكييف التي تعمل بالطاقة الشمسية هي التوافق بين الطلب على التبريد وتوفر الطاقة الشمسية خاصة في المناطق الحارة مثل العراق والتي تحتوي على إمكانيات هائلة للطاقة الشمسية خاصة في فصل الصيف.

النتائج التي تم الحصول عليها تشير إلى إمكانية استخدام الطاقة الشمسية لتقليل الصرف في الطاقة الكهربائية لتطبيقات تكييف الهواء. فالحيز معين يتطلب حمل تبريد مقداره 5 طن (17.5 كيلو واط) وبظروف مناخية (شدة الإشعاع الشمسي 1000 واط لكل متر مربع ودرجة حرارة الجو 45 درجة سيليزية) فان مجمع شمسي بمساحة 40 متر مربع يستطيع أن يوفر 75 % من الحرارة المطلوبة لإنتاج هذا الحمل ومجمع بمساحة 53 متر مربع يستطيع أن يوفر 100 % من الحرارة المطلوبة لإنتاج حمل التبريد المذكور لهذه الظروف المناخية.

1. Introduction

During the last few decades, the consumption of fossil fuel associated with the over loading of the electricity grid for air conditioning purposes, especially at peak demand periods in hot summer increased dramatically in several countries especially in hot climate regions.

Insuring the appropriate comfort conditions for cooling purposes in summer season is one of the main future applications of solar energy especially in regions which enjoy with reasonable higher rates of solar intensity on long period of the year such as in Iraq. During the summer the demand for electricity greatly increases because of the extensive use of air conditioning systems, which increase the peak electric load, causing major problems in the country's electric supply.

The interest in absorption refrigeration systems has increased in recent decades due to the possibility of using weast heat from gas and steam turbines or renewable energies, solar energy in this case, to reduce the consumption of electricity. In addition, they do not contribute to the ozone depletion.

Due to synchronization between the availability of solar energy and need for cooling in hot regions. The use of solar energy to derive absorption cycles for air conditioning of most buildings is an attractive concept.

There are many researchers in literature studied the feasibility of using solar assisted AC systems. Salman Ajib, (2001) [1] analyzed the use of solar thermal energy to operate the absorption refrigeration machine and compare between the absorption and vapor - compression refrigeration machines. He found that, the solar thermal refrigeration systems can be realized and preferred especially in countries with high available resources of sun radiation and a great need for air conditioning. Moncef B. et al, (2005) [2] presented a project aims at assessing the feasibility of solar powered absorption cooling technology under Tunisian conditions. They used (TRNSYS) program to do the simulation. They found that, the absorption solar air conditioning systems are suitable for Tunisian conditions. Marderos A. S. (2007) [3] investigated the theoretical behavior of thermal parameters and their interaction on

absorption cooling system for a climatic condition of Aleppo city in Syria. He found that it is suitable to install solar assisted absorption cycle of AC system in climatic conditions such as that of Aleppo city. Z. sayadi et al, (2010) [4] analyzed the feasibility and economic performance of a solar - assisted AC system for a middle house under the climatic conditions of Tunis city. They found that, 30 m^2 of evacuated tube collector area with a thermal storage tank of about 1 m^3 can cover 87% of the energy needs of a water cooled machine with cooling capacity of 10 kW. Garcia et al, (2011) [5] studied the global modeling of an absorption system working with LiBr - H_2O assisted by solar energy for air conditioning a classroom in Puerto lumbreras, Murcia, Spain. They developed several models for the characterization of the absorption equipment. Their results showed that, the network model predicts with a fair efficiency the value of outlet temperatures and the prediction of COP is not so accurate. AL – Dadah et al, (2011) [6] made experimental work on a solar assisted vapor absorption AC system using propane as a refrigerant and Alkylated benzene (AB300 refrigeration lubrication oil) as absorbent. They found that, the coefficient of performance of the system increases with increasing the generator temperature.

In this paper an investigation has been made to analysis the solar energy powered absorption air conditioning system under the climatic conditions of Iraq. And the effect of most affected parameters has been studied.

2. Absorption VS compression refrigeration system

The vapor absorption refrigeration system is one of the oldest methods of producing refrigeration effect. The principle of vapor absorption was first discovered by Michael Faraday in 1824 [7].

The vapor absorption system uses heat energy instead of mechanical energy as in vapor compression systems in order to change the conditions of the refrigerant required for the operation of the refrigeration cycle. In the absorption system, the compressor is replaced by an absorber, a pump, a generator and pressure reducing valve [8].

3. Lithium bromide - water absorption system

The working principle of an absorption system is similar to that of a vapor compression machine with respect to the key components (evaporator and condenser). The refrigerant (water) evaporates in the evaporator producing the useful cooling effect (Q_{ev}). The water vapor flows to the absorber which can be air or water cooled, in the latter case a cooling tower is necessary to keep the cooling process going. The dilute salt solution exiting the absorber is

pumped through the regenerative solution heat exchanger where it is pre- heated in the generator, so that refrigerant vapor is released. The concentrated solution flow back to the absorber. The desorbed refrigerant condenses in the air or water cooled condenser. The condensate is passed thereafter through an expansion valve where its pressure is so reduced as to provoke its partial evaporation causing a substantial decrease of its temperature. The refrigerant flows finally in the evaporator to complete the evaporation.

4. Mathematical formulation of solar assisted air conditioning system

In solar energy assisted AC system the required heat for separate the solution in generator is taken from a solar collector as a hot water. Following is the mathematical formulation for complete system (hate plate solar collector and LiBr- water absorption cycle) which is shown in Figure (1) .

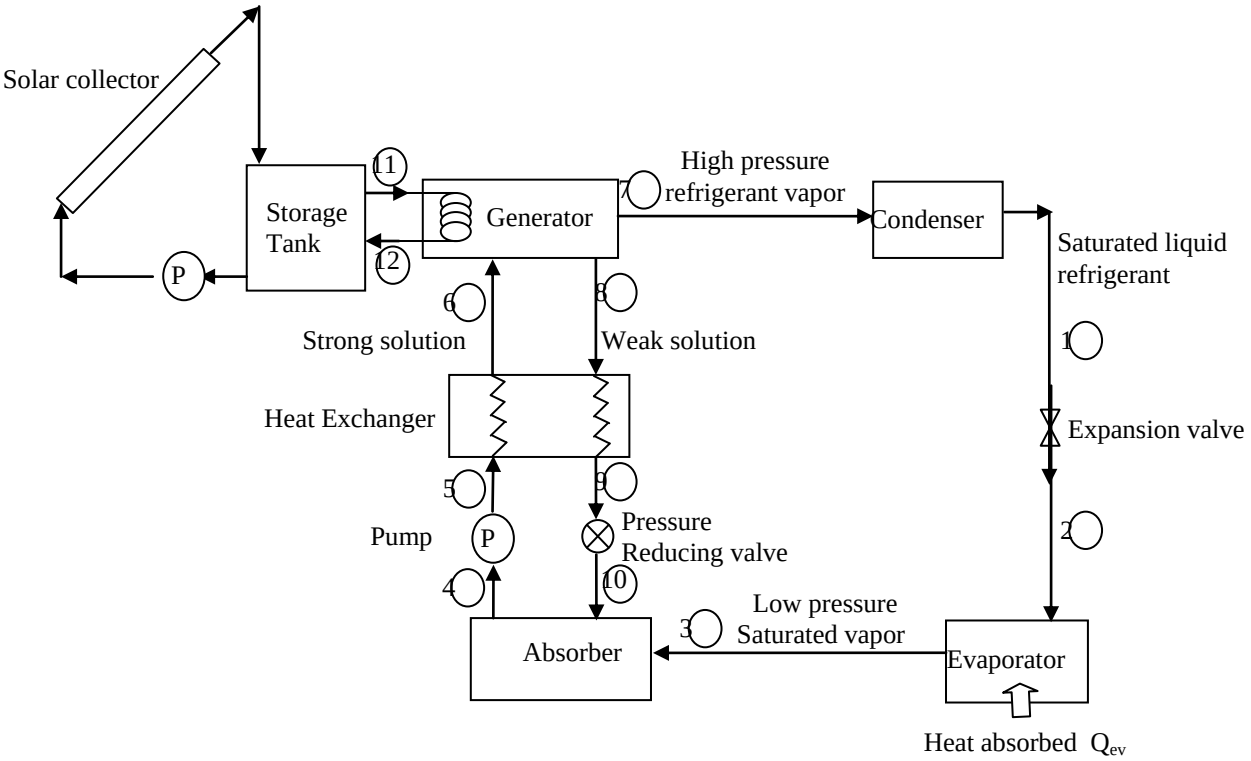

Figure (1). Solar powered air conditioning system.

4-1. Solar collector

Flat plate collectors are most widely used in this type of applications. For a flat plate solar collector with coefficient of transmittance - absorbency ($\alpha\tau = 0.79$) and ($Fr = 0.75$), the overall heat transfer coefficient of the collector ($U = 6$ W/m^2.C^o) [2][3].

The solar collector efficiency [3]:

$$\eta_{coll} = Fr \times [(\alpha\ \tau)\ -\ \frac{U_{coll}\,(Tin - Tamb)}{I_s}] = \frac{Q_{ucoll}}{I_s\,A_{coll}} \quad (1)$$

Where:

T_{in} is the temperature of water input to the collector, T_{amb} is the ambient temperature, I_s is the solar radiation intensity, A_{coll} is the total area of the solar collector, Q_{ucoll} is the useful heat from the solar collector.

$$Q_{ucoll} = m_{coll}\ Cp_w\ (T_g - T_{in}) \quad (2)$$

This heat is supplied to the generator and T_g is the temperature of water exit the collector (generator temperature).

4-2. Absorption refrigeration cycle

The first step of absorption cycle calculations is to specify and calculate the conditions of all points in the cycle (temperature, pressure, enthalpy, flow rate and concentration of solutions). Then the heat exchanged with ambient through four main components (generator, condenser, evaporator and absorber) can be calculated by the following equations:

Evaporator:

$$Q_{ev} = m_3h_3 - m_2h_2 \quad (3)$$

Where $m_2 = m_3$

Absorber:

$$Q_{ab} = m_3h_3 + m_{10}h_{10} - m_4h_4 \quad (4)$$

$$m_3 + m_{10} = m_4 \quad (5)$$

Condenser:

$$Q_{cond} = m_1h_1 - m_7h_7 \quad (6)$$

Where: $m_1 = m_7$

Generator:

$$Q_g = m_7h_7 + m_8h_8 - m_6h_6 \quad (7)$$

$$Q_g = Q_{ucoll} = m_{coll}\ Cp_w\ (T_g - T_{in}) = m_{coll}\ Cp_w\ (T_{12} - T_{11}) \quad (8)$$

For heat exchanger, the effectiveness can be expressed as follow:

$$\epsilon = \frac{Q_{act}}{Q_{max}} = \frac{Q_{act}}{(mcp)_{min}\,(T_{hi} - T_{ci})} \quad (9)$$

$$Q_{act} = (mCp)_c\,(T_{co} - T_{ci}) = (m\,Cp)_h\,(T_{hi} - T_{ho}) \quad (10)$$

For $(mCp)_{min} = (mCp)_c$

$$\epsilon = \frac{(mCp)_c\,(T_{co} - T_{ci})}{(mCp)_c\,(T_{hi} - T_{ci})} = \frac{(T_{co} - T_{ci})}{(T_{hi} - T_{ci})} \quad (11)$$

Where $T_{co} = T6$, $T_{ci} = T5$, $T_{hi} = T8$, $T_{ho} = T9$

$$T6 = T5 + \epsilon\,(T8 - T5) \quad (12)$$

The coefficient of performance of the cycle:

$$COP = \frac{Q_{ev}}{Q_g + w_p} \quad (13)$$

Where w_p is the power consumption in small pump used to circulate the solution. By neglecting w_p due to its small value, the coefficient of performance become [3, 4]:

$$COP = \frac{Q_{ev}}{Q_g} \quad (14)$$

4-3. Solar air conditioning system

Thermal efficiency of the solar cooling system determined by parameter called solar thermal ratio (STR) which represents the overall efficiency of the system:

$$STR = COP \times \eta_{coll} \quad (15)$$

Solar contribution (f) can be calculated from [3],[9]:

$$f = \frac{Q_{ucoll}}{Q_{ev}}\,COP \quad (16)$$

When the solar energy is insufficient to operate the system, auxiliary heater must be used to provide the required heat. The auxiliary heater contribution (H_{aux}) can be calculated from:

$$H_{aux} = 1 - f \quad (17)$$

5. Results and discussion

As mentioned before the absorption cycle needs heat energy to change the condition of refrigerant to produce refrigeration effect. The heat is supplied to the generator to increase its temperature to separate the solution.

Figure(2) shows the variation of generator temperature with collector area for three values of solar radiation intensity (700, 900 and 1000 W/m2) at ambient temperature 45 ^{o} C. From this Figure it can be seen that, the temperature of generator increases with increasing the area of collector for all values of solar radiation due to increase the amount of heat collected with increasing the area of collector which leads to increase the heat transferred to the generator. Also it can be noted from this Figure that, the generator temperature increases with increasing the solar radiation intensity as a result of increasing the amount of heat transfer.

Figure(3) indicates the variation of generator temperature with area of collector for selected values of ambient temperature at solar radiation 1000 W/m^2. From this Figure one can observe the increasing of generator temperature with increasing the area of collector for all values of ambient temperature due to increasing the heat transfer as explained in previous Figure. Also the increment in generator temperature for different values of ambient temperature is increased with increasing collector area.

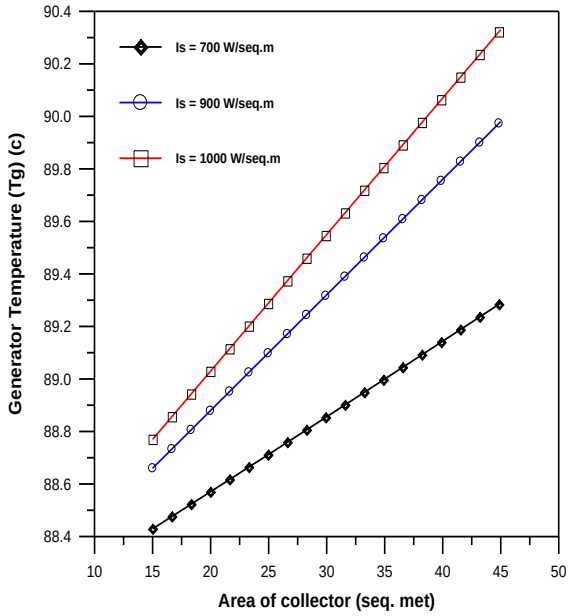

Figure(2). Variation of generator temperature with area of collector for T_{amb} = 45 C^o.

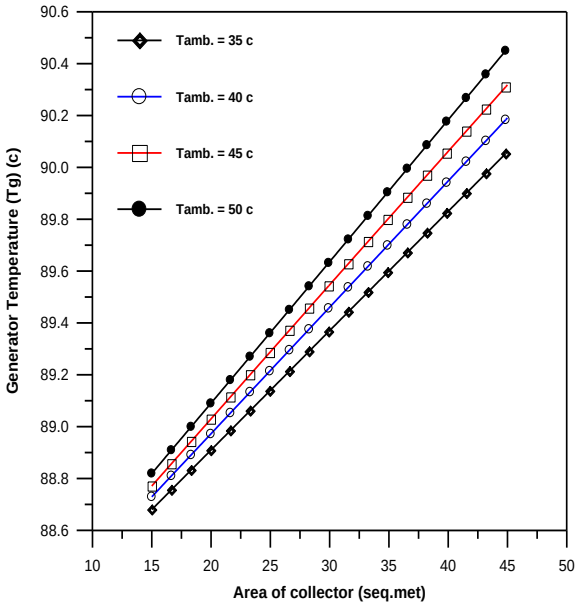

Figure (3). Variation of generator temperature with area of collector for Is =1000 W/m^2.

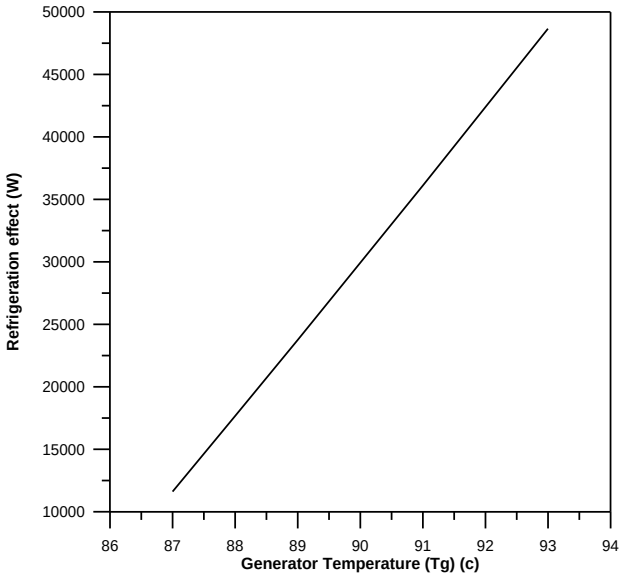

Figure (4). Variation of cooling effect (Q_{ev}) with generator temperature .

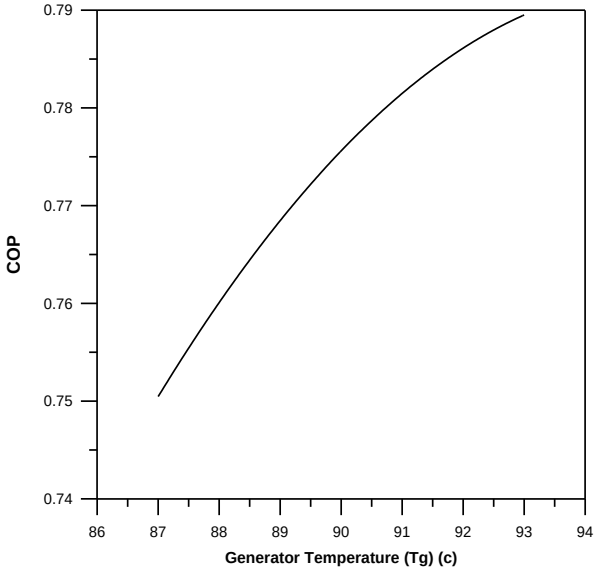

Figure (5). Variation of coefficient of performance with generator temperature .

Variation of cooling effect of the system with generator temperature is presented in Figure (4). From this Figure it can be seen that, the capacity of system is increased with increasing the generator temperature due to increase the efficiency of separation process occurred in generator which lead to maximize the absorption process in the absorber and as a result produce extra circulation for the solution and increasing the flow rate of refrigerant, therefore the heat absorption process in evaporator is increased.

Figure (5) shows the variation of coefficient of performance with generator temperature. From this Figure one can see that, the coefficient of performance is increased with increasing the generator temperature due to increase the heat absorbed in evaporator (cooling effect) as discussed in previous paragraph.

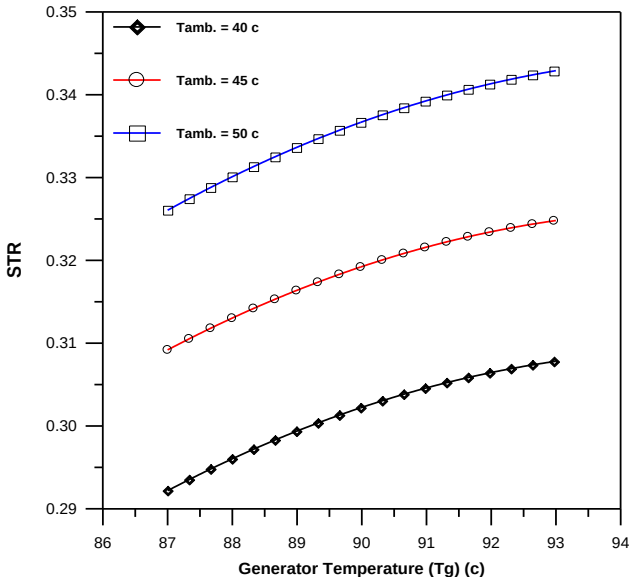

Figure (6). Variation of solar thermal ratio with generator temperature at Is =1000 W/m^2

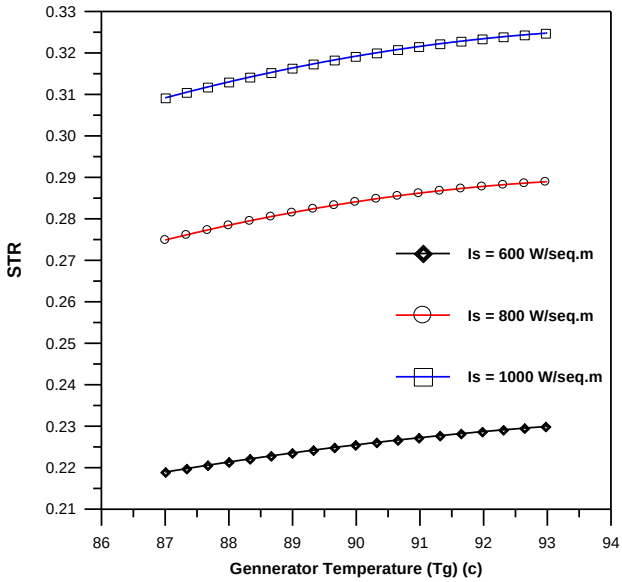

Figure (7). Variation of solar thermal ratio with generator temperature at T_{amb} =45 ^{o}C

Figure (6) shows the variation of solar thermal ratio (STR) with generator temperature for selected values of ambient temperature at (Is =1000 W/m^2). The results presented in this Figure refer to increase of solar thermal ratio which represents the overall efficiency of solar air conditioning system with increasing the generator temperature for all values of ambient temperature due to increase the coefficient of performance of absorption cycle with increasing generator temperature. Also it can be seen that, the STR is increased with increasing the ambient temperature due to increase the efficiency of solar collector and collecting extra amount of heat.

Figure (7) represents the variation of STR with generator temperature for different values of solar radiation intensity at T_{amb} = 45 ^{o}C. From this Figure one can see that, the STR values is increased with increasing the generator temperature for all selected values of solar radiation due to increase the coefficient of performance. The STR is also increased with increasing the solar radiation due to increase the efficiency of solar collector and the amount of heat transferred.

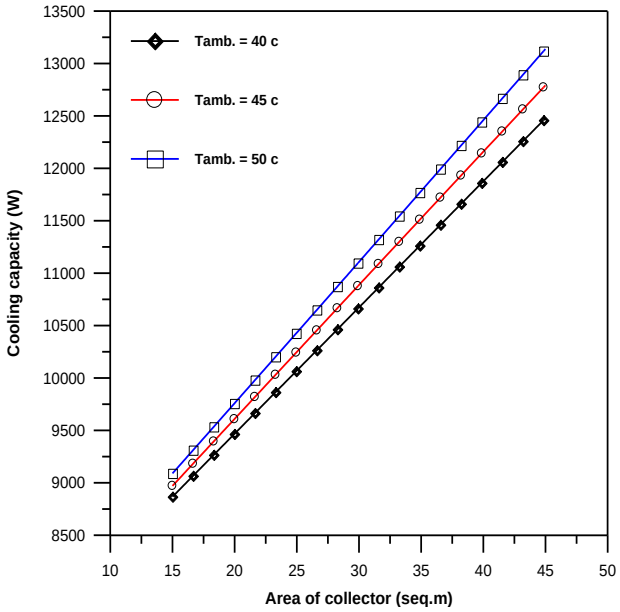

Figure (8). Variation of cooling effect with collector area at Is =1000 W/m^2.

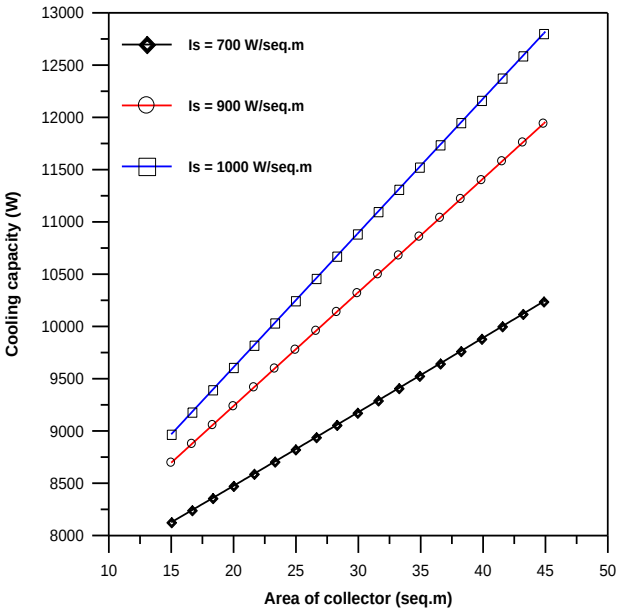

Figure (9). Variation of cooling effect with collector area at T_{amb} =45 C^{o}.

Variation of cooling capacity of the system with collector area for different values of ambient temperature at (Is =1000 W/m^2) is shown in Figure8. From this Figure it can be seen that the cooling capacity is increased with increasing the area of collector for all values of ambient temperature as a result of increasing the heat absorbed in collector which lead to increase the efficiency of absorption process and enhance the refrigerant flow rate. Also there is increase in cooling effect with increase the ambient temperature for the same collector area due to increase the heat absorbed.

Figure (9) indicates the variation of cooling capacity of the system with collector area for different values of solar radiation at (T_{amb} = 45^{o} C). From this Figure the cooling capacity increased with increase the collector are for all values of solar radiation due to increase the amount of heat collected in the collector which lead to improve the absorption process and enhance the refrigerant flow rate. The cooling effect is increased also with increase the solar radiation due to increase the heat absorption.

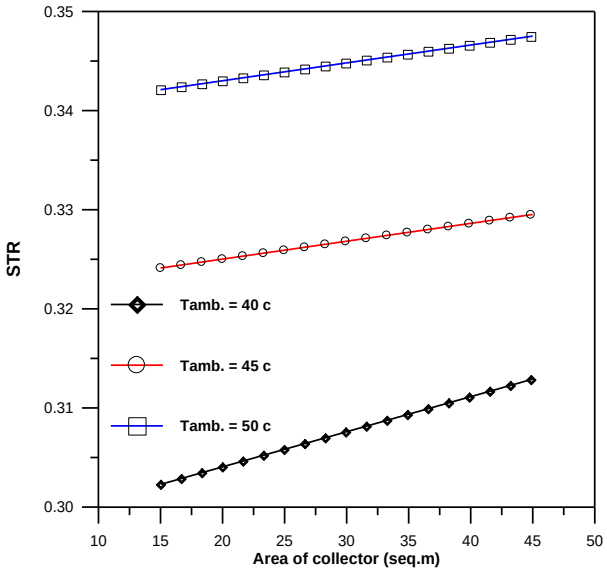

Figure (10). Variation of solar thermal ratio with collector area at Is =1000 W/m^2.

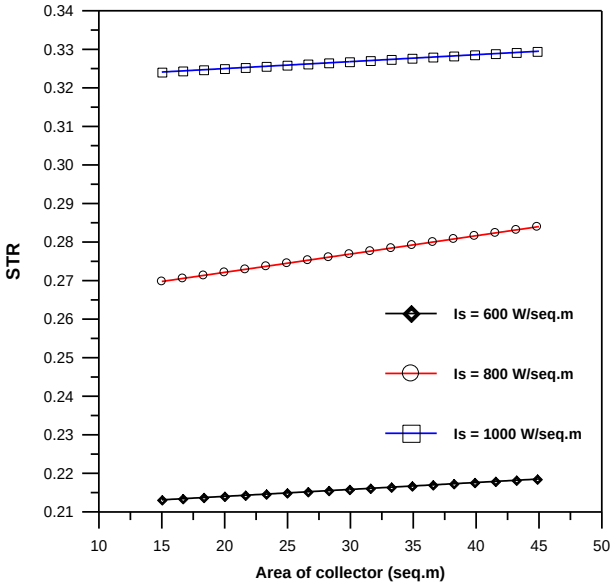

Figure (11). Variation of solar thermal ratio with collector area at T_{amb} =45^o C.

Figure (10) represents the variation of STR with collector area for different values of ambient temperature at (Is =1000 W/m^2). From this figure it can be seen that, STR is increased with increasing collector area for all values of ambient temperature due to increase the efficiency of the heat collecting and absorption processes. Also STR increased with increasing the value of ambient temperature due to increase the thermal efficiency of solar collector. Variation of STR with collector area for different values of solar radiation at (T_{amb} = 45^o C) is presented in Figure(11). The results presented in this Figure indicate that, STR is increased with increasing the area of collector for all values of solar radiation as discussed in Figure (10). Also STR is increased with increasing the solar radiation due to increase the efficiency of collector and increases the heat collecting.

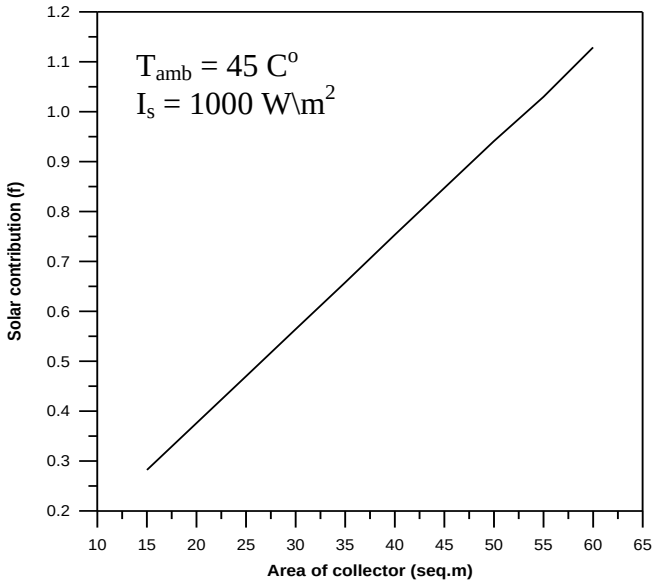

Figure (12). Variation of solar contribution with Collector area.

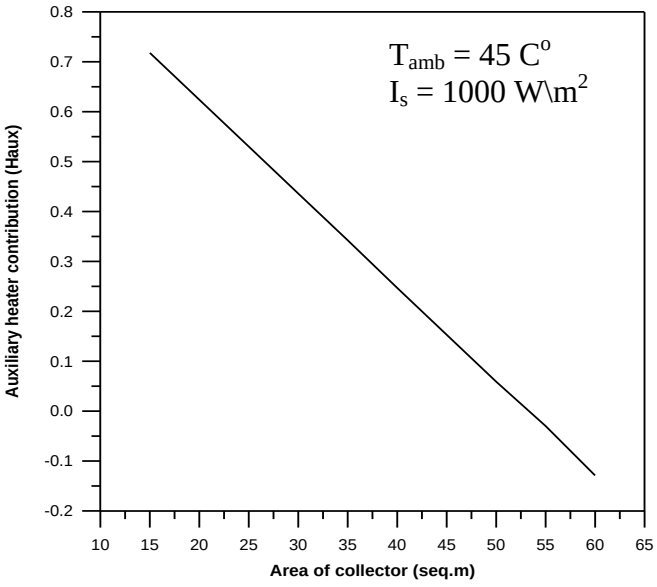

Figure (13). Variation of auxiliary heater contribution with Collector area .

Figure (12) shows the variation of solar contribution with area of collector for a certain space with cooling load demand 5 Ton at weather conditions (T_{amb} = 45^{o} C and Is =1000 W/m^2). From this Figure it can be seen that, the solar contribution is increased with increasing the area of collector due to increase the heat collection process and as a result the absorption process is increased. As can be seen from this figure a solar powered air conditioning system with collector area 53 m^2 at the mentioned weather conditions can produce the required cooling load and producing extra cooling load require extra area for collector. The results presented in this Figure indicate that, the coupling of absorption refrigeration machines and solar energy can be adequately used to produce the cooling demand for moderate residential applications using solar collectors with reasonable area.

Figure (13) indicates the variation of auxiliary heater contribution with collector area for the same cooling load and climatic conditions mentioned in Figure (12). The auxiliary heater used in this system to store the extra unneeded heat produced by solar collector and give this heat to the air conditioning system in time where the solar energy is insufficient or unavailable. From this Figure one can observe that, the auxiliary heater contribution is decreased with increasing the collector area, since with increasing the collector area the solar contribution is increased and the needing for auxiliary heater is vanished.

6. Conclusions

In this paper an investigation was made to study and analyzes the solar assisted absorption air conditioning systems. From the results obtained the following conclusions can be achieved:

1- Solar energy can be used efficiently to provide the heat required to operate the absorption air conditioning systems to produce required cooling for small residential applications.
2- The coupling of solar collectors and absorption refrigeration machines is able to reduce the power consumption for air conditioning applications for hot regions due to the synchronization between cooling demand and availability of solar energy.
3- The area of collector and weather conditions play an important role to increase the cooling capacity of the system.
4- The solar powered AC systems need extra research work to find out the optimum values of affecting parameters and other types of solar collectors must be studied to find out the effect of type of solar collector on the performance of this system.

5- The only disadvantage of this system is its need for large surface area of solar collector.

7. References

[1] Salman Ajib, "profitability of using solar energy for refrigeration and air conditioning", IEEE, 2001

[2] Moncef B., Mohamed H.C., Amenallah G., "Solar powered air conditioning as a solution to reduce environmental pollution in Tunisia", Desalination, 185, pp. 105 – 110, Elsevier, 2005.

[3] Marderos A.S, "The solar contribution to air conditioning systems for residential buildings", Desalination, 209, p.p 171-179, Elsevier, 2007.

[4] Sayadi z., S., El may, mohamoud B., A. Bellagi, "Technical and Economic analysis of solar- assisted air- conditioning system", Thermal Issues in Emerging Technologies, THETA3, Cairo, Egypt, Des. 19 - 22nd, 2010.

[5] Garcia c., F. vera G., JM. CanoI.J.P. Delgado M.,R. Martinez S.," modeling an absorption system assisted by solar energy", Journal of Applied Thermal Engineering, 31, pp. 112 - 118, Elsevier, 2011.

[6] AL-Dadah R.K.,G. Jackson, Ahmed R., "solar powered vapor absorption system using propane and alkylated benzene AB300011", Journal of Applied Engineering, 31, pp 1936 - 1942, Elsevier, 2011.

[7] Abbas A.S. AL- Jeebori, "fundamentals of air conditioning and refrigeration", first edition, AL- Qadisiya university, 2006.

[8] Edward G. pita, "Air conditioning principles and systems", fourth edition, prentice- Hall if India, 2005

[9] Rodriguez M. C. H., P. Rodriguez A.,M. Izquierdo M.,A. Lecuona N., R. Salgado M., "Energy and carbon emission saving is Spanish housing air- conditioning using solar driven absorption system", J. of Applied thermal Engineering 28, pp. 1734 - Elsevier 2008.

[10] Antonio P.F., Francisco A. B., Moacir M.M, Dougas B.R., "central air conditioning based on adsorption and solar energy" J. of Applied thermal Engineering 31, pp.50 - 58, Elsevier, 2011.

8. Nomenclature

symbol	Description	SI unit
A_{coll}	Total area of collector	m^2
COP	Coefficient of performance	-
Cp	Specific heat	$J/kg.C^o$
f	Solar contribution	-
h	enthalpy	kJ /kg
H_{aux}	Auxiliary heater contribution	-
I_s	Solar radiation intensity	W/m^2
m	Mass flow rate	kg/s
Q_{ucoll}	Useful heat from solar collector	w
T	Temperature	C^o

Greek letters

Symbol	Description	SI unit
η_{coll}	Collector efficiency	-
ε	Heat exchanger effectiveness	-

Subscripts

symbol	Description
ab	absorber
act	actual
amb	ambient
c	cold
coll	collector
cond	condenser
ev	evaporator
g	generator
h	hot
in	inlet
max	maximum
min	minimum
o	outlet

A New Differential Configuration of Hybrid Electric Vehicle with Torque Regulationloop

Abdul baki Khalaf Ali
Mechanical Engineering Department
College of Engineering
University of Basrah
Basrah, Iraq
westofbas@yahoo.com

Basil Sh .Munahi
Mechanical Engineering Department
College of Engineering
University of Basrah
Basrah, Iraq
basilaljorani@yahoo.com

Karrar Abbas Johi
Mechanical Engineering Department
College of Engineering
University of Basrah
Basrah, Iraq
Karrar_engd@yahoo.com

Imad abdul-kadhem kheioon
Mechanical Engineering Department
College of Engineering /University of Basrah
Basrah, Iraq
phdimad@yahoo.com

Abstract

The most significant weakness of hybrid electric vehicles (HEV) is the high construction cost and the complicated control strategies due to multiple power sources[1],[2] .In this paper a new developed configuration of hybrid vehicle is presented. The new configuration is simple, cost-effective and easy to implement .The differential unit, which acts as mechanical torque-overflow keeps engine torque within a predefined value . This is achieved by the aid of torque loop attached to one terminal of the differential.The new configuration proved to act continuously varying transmission (CVT) and also can perform efficient control strategies . Minimum emissions can be assured by running the IC-engine within best engine performance zone which is characterized by engine torque and engine speed.

KEYWORDS : Hybrid electric vehicle (HEV), torque loop, control strategy, continuously varying transmission (CVT).

بناء نموذج تفاضلي جديد من المركبات الكهربائية الهجينة مبني على أساس تنظيم العزوم الدوارة

المستخلص

أن من ابرز نقاط الضعف في المركبات الكهربائية الهجينة هي كلفة الإنشاء العالية والتعقيد في استراتيجيات السيطرة بسبب تعدد مصادر القدرة. تم في هذا البحث بناء نموذج جديد من المركبات الهجينة. يمتاز هذا النموذج بالبساطة وقلة الكلفة وسهولة التنفيذ. أن الوحدة الأساسية وهي الوحدة التفاضلية والتي تعتبر بمثابة الطوافة للسيطرة على العزوم الزائدة

للمحرك ولإبقاء عزم المحرك ضمن القيم المرغوبة والمعرفة سلفا للنموذج. يتم كل ذلك بمساعدة مسار التحكم بالعزم والمسيطر على احد أطراف الوحدة التفاضلية. لقد اثبت النموذج الجديد بأنه يوفر (مغير سرعة مستمر) ومسيطر جيد على المركبات الهجينة. ان النموذج الجديد يضمن كذلك تقليل الانبعاثات الملوثة عن طريق تشغيل محرك الاحتراق ضمن منطقة الأداء الأفضل ضمن مخطط السرعة والعزم للمحركات .

1. Introduction

A HEV is a hybrid electric vehicle in which propulsion energy is available from two or more kinds or types of energy stores, sources or converters, and at least one of them can deliver electrical energy[1] .

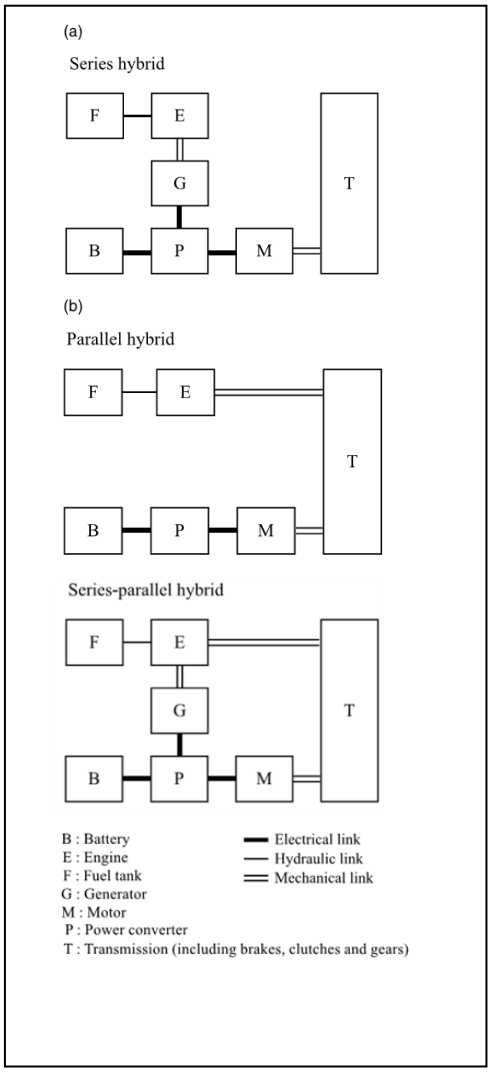

Figure (1). Classifications of HEV .

Traditionally, HEVs were classified into two basic kinds—series and parallel. Recently, with the introduction of some HEVs offering the features of both the series and parallel hybrids, the classification has been extended to[1]:

• series hybrid,

• parallel hybrid,

• series–parallel hybrid, and

• complex hybrid.

The complex hybrid is a complicated mix of either type of hybrid models .

2. Series hybrid system (SHEV)

The series hybrid is the simplest kind of HEV .Its engine mechanical output is first converted into electricity using a generator .The converted electricity either charges the battery or can bypass the battery to propel the wheels via the same electric motor and mechanical transmission .Conceptually, it is an engine-assisted EV which aims to extend the driving range to be comparable with that of the ICEV .Because of the absence of clutches throughout the mechanical link, it has the definite advantage of flexibility for locating the engine-generator set .Although it has an added advantage of simplicity of its drive train, it needs three propulsion devices—the engine, the generator and the electric motor .Another disadvantage is that all these propulsion devices need to be sized for the maximum sustained power if the series HEV is designed to climb a long grade .On the other hand, when it is only needed to serve such short trips as commuting to work and shopping, the corresponding engine-generator set can adopt a lower rating[1].

3. Parallel hybrid electric vehicles (PHEV)

In PHEV, both the mechanical power output and the electrical power output are connected in parallel to drive the transmission as shown in Figure (1-a) .There are various control strategies used for parallel configuration .In the most common strategy, ICE is basically always in on mode and operates at almost constant power output at maximum efficiency point [2]Electric motor is tuned on when the power from the ICE is less than that required by the transmission .The electric motor can be used as a generator to charge the

battery by regenerative braking or absorbing power from the engine when its output is greater than that required to drive the wheels.

4. Series-parallel hybrid system (SPHEV)

In the series-parallel hybrid, the configuration incorporates the features of both the series and parallel HEVs, but involves an additional mechanical link compared with the series hybrid and also an additional generator compared with the parallel hybrid .Although possessing the advantageous features of both the series and parallel HEVs, the series-parallel HEV is relatively more complicated and costly .Nevertheless, with the advances in control and manufacturing technologies, some modern HEVs prefer to adopt this system.

5. The complex hybrid system (CHEV)

As reflected by its name, this system involves a complex configuration which cannot be classified into the above three kinds . The complex hybrid seems to be similar to the series-parallel hybrid, since the generator and electric motor are both electric machinery .However, the key difference is due to the bidirectional power flow of the electric motor in the complex hybrid and the unidirectional power flow of the generator in the series-parallel hybrid.This bidirectional power flow can allow for versatile operating modes, especially the three propulsion power (due to the engine and two electric motors)operating mode, which cannot be offered by the series-parallel hybrid .Similar to the series-parallel HEV, the complex hybrid suffers from higher complexity and costliness.Nevertheless, some newly introduced HEVs adopt this system for dual axle propulsion [1].

The new differential model with torque– loop

Figure (2) shows the new developed model .The differential

block, shown in hatched square represents the main linking unit .It links three power devices these are :IC engine-connected at shaft (B), DC generator connected to shaft (F1) and DC motor connected

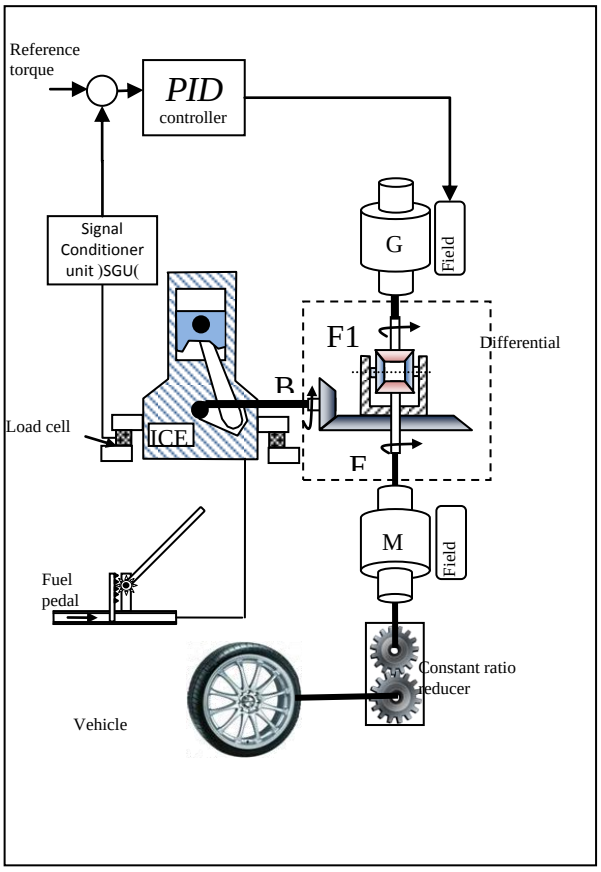

Figure (2). New differential model with torque– loop.

to shaft (F2). The DC motor is connected to the vehicle wheels either directly or by means of gear reducer . The other important thing to notice in this new configuration is the torque loop. Many researchers interested in torque control for hybrid electric vehicles [3]. The torque signal is generated by the load cell attached to the engine supports . The signal is conditioned then through an electronic circuit to be compared with a predefined value namely the reference torque. The result of comparison is fed to a well tuned PID controller to produce a suitable field voltage for the DC generator .The field voltage of the DC motor is considered to be fixed to the rated value. The driver has only one variable to control the vehicle with .It is the fuel pedal .As he pushes the pedal, engine speed increases . Generator speed is also increased the torque loop pushes an amount of field voltage to the generator .This amount is exactly the amount that produces a certain torque .Regulating the generator torque which is connected to on terminal of the differential leads to regulate the torque of IC-engine because all the terminal of the differential has constant torque relation . This model succeed to run the engine at its rated torque .The main blocks are described below:

The differential block

Figure (3) shown represents the differential block .The input shaft is to be shaft (B1)while the output shafts are (F1) and (F2).

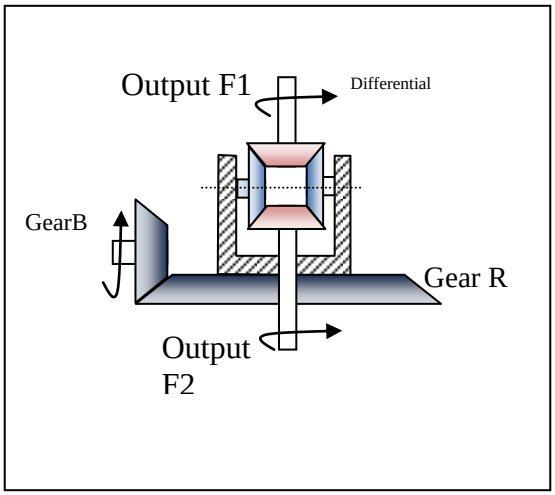

Figure (3) .The differential block.

The gear ratio between gear (R) and gear (B) is G_D . The speed relationship is [4]:

$$N_B = \frac{G_D}{2}(N_{F1} + N_{F2}) \quad (1)$$

This means that the speed is divided between (F1) and (F2) in a differential manner .

The torque relationship is given by:

$$T_{F1} = T_{F2} = G_D T_B \quad (2)$$

One can note that the torques of the three terminal of the differential block are linearly related . If any of the three terminals is released then the torque for all terminals will equal zero i.e. , that is, the lowest torque terminal will control the torque value of the block . Referring to Figure (2) :

$$T_G = G_D T_{IC} \quad (3)\text{Or}$$

$$T_{IC} = \frac{1}{G_D} T_G \quad (4)$$

So regulating the value of generator torque (T_G) led to regulating the value of IC engine torque (T_{IC}).

The DC machines

The general form for the torque on any Dc machine is given by[5]:

$$T = K_1 \emptyset I_a \quad (5)$$

$$T = K_2 I_f I_a \quad (6)$$

Where I_a is armature current and $\emptyset$ is the magnetic flux.

The generated back emf (E_b) is given by:

$$E_b = K_3 \emptyset N \quad (7)$$

$$E_b = K_4 I_f N \quad (8)$$

Where N is the speed of the machine.

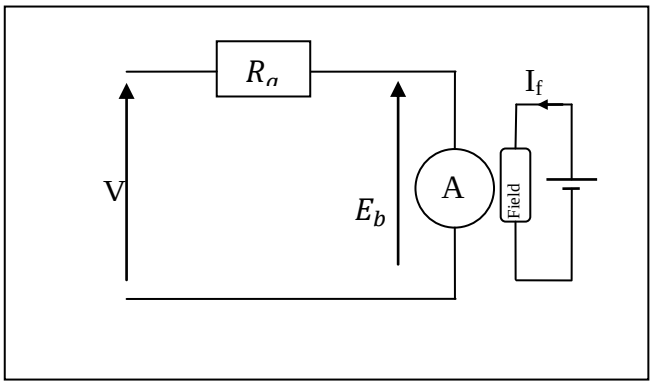

Figure(4). DC machine.

For the set of generator-motor

The current passing through both armatures as shown in Figure (5) is given by :

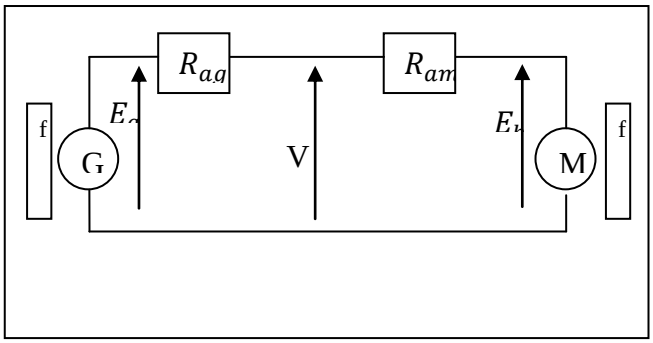

Figure (5). Generator-motor set.

$$I_a = \frac{E_a - E_b}{R_{ag} + R_{am}} \quad (9)$$

$$I_a = \frac{K_4 I_{fg} N_g - K_4 I_{fm} N_m}{R_{ag} + R_{am}} \quad (10)$$

Where :I_{fg}, I_{fm} is the field currents of generator and motor respectively.

N_g, N_m are the speeds of generator and motor respectively.

$R_{ag}, R_{am}$are the armature resistance of generator and motor respectively.

$$T_m = K_2\, I_{fm} I_a = K_2\, I_{fm} \frac{K_4 I_{fg} N_g - K_4 I_{fm} N_m}{R_{ag} + R_{am}}$$

All K_2, K_4, R_{ag}, and R_{am} are constants

$$T_m = K_6\, I_{fm}(I_{fg} N_g - I_{fm} N_m) \quad (11)$$

Similarly for generator :

$T_g = K_2\, I_{fg} I_a$

$$T_g = K_6 I_{fg}(I_{fg} N_g - I_{fm} N_m) \quad (12)$$

For the hybrid configuration of Figure (2),

$$T_g = K_6 I_{fg}(I_{fg} N_g - I_{fm} N_m) = T_{ref}$$

$$(I_{fg} N_g - I_{fm} N_m) = \frac{T_{ref}}{K_6 I_{fg}}$$

$$T_m = \frac{I_{fm}}{I_{fg}} T_{ref} \quad (13)$$

For similar machines (similar field impedance)

$$T_m = \frac{V_{fm}}{V_{fg}} T_{ref} \quad (14)$$

Where V_{fm}, V_{fg} are field voltages of generator and motor respectively.

To solve for I_{fg}, let the electrical torque gain (γ) equal :

$$\gamma = \frac{T_m}{T_g} = \frac{I_{fm}}{I_{fg}} = \frac{V_{fm}}{V_{fg}} \quad (15)$$

or

$$I_{fm} = \gamma I_{fg}$$

Substitute in Eq. (12) gives:

$T_g = K_6 I_{fg}(I_{fg} N_g - I_{fm} N_m) = T_{ref}$

$T_g = K_6 I_{fg}(I_{fg} N_g - \gamma I_{fg} N_m) = T_{ref}$

$T_g = K_6 I_{fg}^2(N_g - \gamma N_m) = T_{ref}$

$$I_{fg} = \sqrt{\frac{T_{ref}}{K_6(N_g - \gamma N_m)}} \quad (16)$$

The speed of top gear is to start at (V_t)

The top gear means that $\gamma = 1$ and :

$$\gamma = \frac{V_t}{V_x} \quad (17)$$

where V_x is vehicle velocity. The motor speed is linearly related to vehicle speed and one can write:

$N_m = C_2 * V_x$ so:

$$V_{fg} = C1\sqrt{\frac{T_{ref}}{(N_g - \gamma C_2 V_x)}} \quad (18)$$

The above formula derived for a differential gain of $G_D = 1$ for values other than 1, it must be included and hence:

$$V_{fg} = C1\sqrt{\frac{G_{D*}T_{ref}}{(N_g - \gamma C_2 V_x)}} \quad (19)$$

Where T_{ref} is the reference torque of the IC engine. Its value depends on the performance map of the engine . At any speed of the IC-engine there is an optimum value for the torque to give highest power and minimum emissions.

Equation (19) is a straightforward relation that gives always a unique value for field voltage of the generator corresponding to the desired reference torque of the IC-engine and the current speed of the generator.

Referring to Figure (2) , the total driving torque T_D is the sum of T_{F2} and T_m , so:

$$T_D = T_{F2} + T_m \quad (20)$$

but

$T_{F2} = G_D T_{IC}$ (Eq.2) and $T_m = \gamma T_g$(Eq.15)

$T_D = G_D T_{IC} + \gamma T_g$

The generator is connected to the terminal F1 of the differential so $T_g = G_D T_{IC}$,

$T_D = G_D T_{IC} + \gamma G_D T_{IC}$

The torque loop tries to regulate the engine torque to its reference value ,$T_{IC} = T_{ref}$ this means:

$$T_D = (G_D + \gamma)T_{ref} \quad (21)$$

Equation (21) summaries all the current work .It shows that the total torque gain is compound of two components :mechanical, G_D , which is constant and electrical , γ, which is variable with vehicle speed . This work shows that there is no further need to change the mechanical gain G_D manually or automatically since it is possible to easily change the value of electrical gain γ .Also it is important to notice that the torque loop which is acting as the watchdog for the torque of the engine , keeps the torque always near its reference value .

The question arises now, will γ be changed automatically or there is a need for manual shifting?

When the vehicle just start to move it needs for large torque gain , the engine tries to move the terminal F1 of the differential but it is heavy to move so the differential flows power to the other easy terminal , F2, which is attached to the generator .The generator starts to speed up and according to Eq.(19), there is always a unique value for V_{fg} that combine all the variable (T_{ref}, N_g, V_x and γ) .This means also that the field voltage of the generator plays this magic role for satisfying vehicle torque and engine torque, and acts together with the torque loop as CVT(continuously varying transmission).

The simulink model

Figure (6) represents the simulink structure of the proposed model.The differential blocks links the gasoline engine with the generator and the motor . The two DC machines are runnig in the speed mode .Shaft sensor block is needed to transform the mechanical link to simulink signal .The torque actuator block is used to transform the simulink torque signal of the motor to mechanical link to be coupled then with the port (F1) of the differential.

The torque loop is started with (T_{ref}). It is important to note that the value of T_{ref} used here is equal to ($G_D * T_{ref}$)of the engine , this is because we measure the torque of the generator not the IC engine .In physical or practical system where it is possible to measure T_{ref} of the engine by attaching load cells to engine base and hence no need to modify by G_D.
A well tuned PID controller is used in this loop together with saturation block to limit the output field voltage to its upper limit.

The gasoline engine used in this structure has 80 kw max power at 2000 rpm and has maximum speed limit of 3000 rpm.

6. Discussions

To show the vehicle capabilities of acceleration and smooth gear shifting during driving scheme, a block of suitable parameters is built . It is the reference speed block . The block assumes that the vehicle accelerates from 0 to 100 km/h (30m/s) at 10 seconds . It watches the vehicle speed and checks if it is coincide with the reference velocity profile . Any error between the reference speed and the actual speed pushes the block to open extra throttle.

This exactly what a human driver do when he want to drive a vehicle. Any drive has its own driving profile .Some have fast profile and other have slow profiles .This block is needed just for simulation to add real time throttle control .In practical case it is not needed since human driver is doing the job.

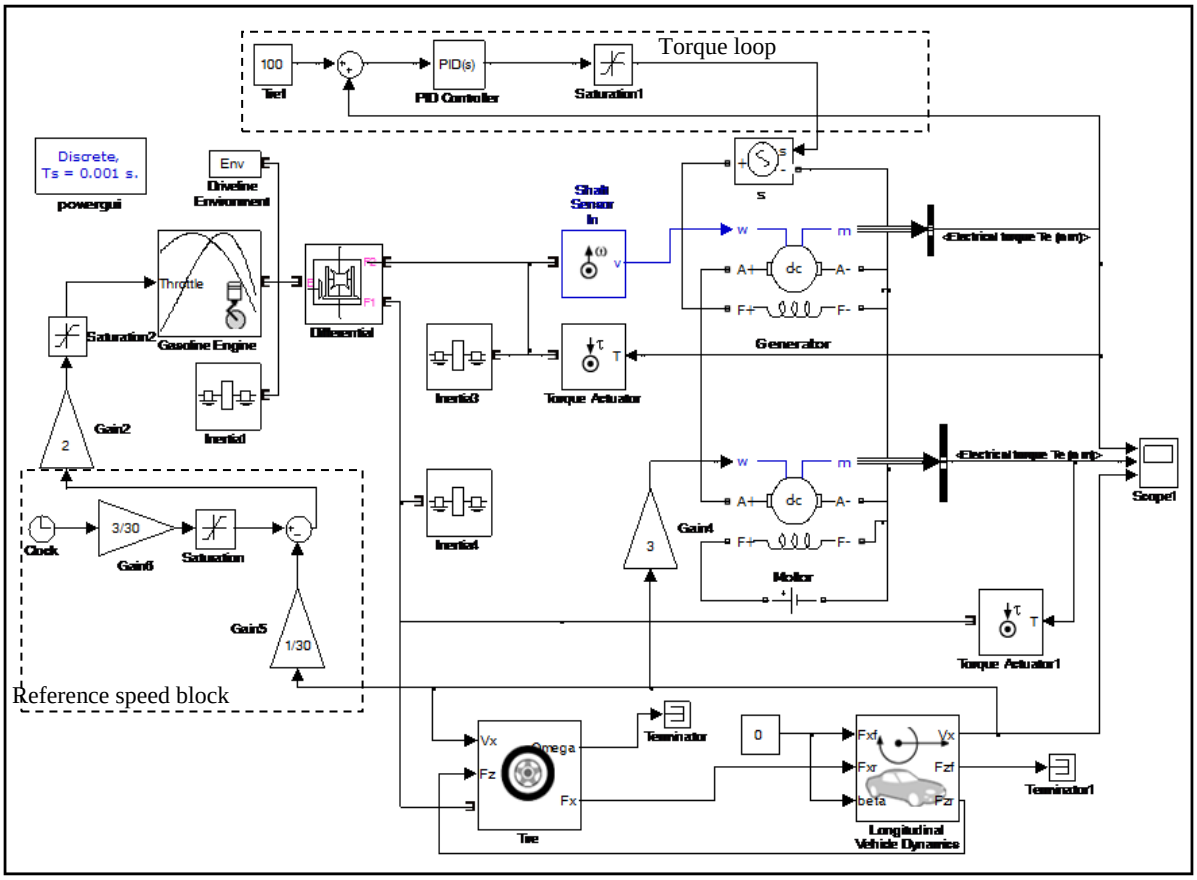

Figure (6). Simulink model .

The longitudinal vehicle dynamics block represents the vehicle . The mass used here is 1400 kg which is a midsized vehicle . Scopes are used whenever needed to monitor a variable.The generator torque is seemed to be regulated at the reference value (which is 100N.m). It is negative because the generator torque is a load against engine torque . The PID controller tries to keep the torque within its reference value . The second graph ,which is the motor torque graph is the most important graph . During the first period of time the torque starts to increase until it become enough to move the vehicle .It reaches its maximum value and then begins to fall as the vehicle speed builds up .At top gear speed the motor torque approximates the generator torque as seen it became asymptote to (100 N.m). The third graph shown in Figure (7) represents the vehicle speed in (m/s) . The top gear speed in this model is 30m/s (around 100km/h). It is also clear that when the vehicle speed reaches the top gear speed the motor torque became equal approximately to generator torque and consequently the electrical torque gain (γ) becomes equal to 1 . The velocity profile of the vehicle coincides with the reference velocity profile, where the vehicle is assumed to accelerate from 0 to top gear speed in approximately linear ramp.It is important to note that as the generator torque is locked to the value of 100 N.m which is ($G_D * T_{ref}$), the engine torque is locked to the value of T_{ref} . This means that it is possible to run the IC engine within the recommended perform.

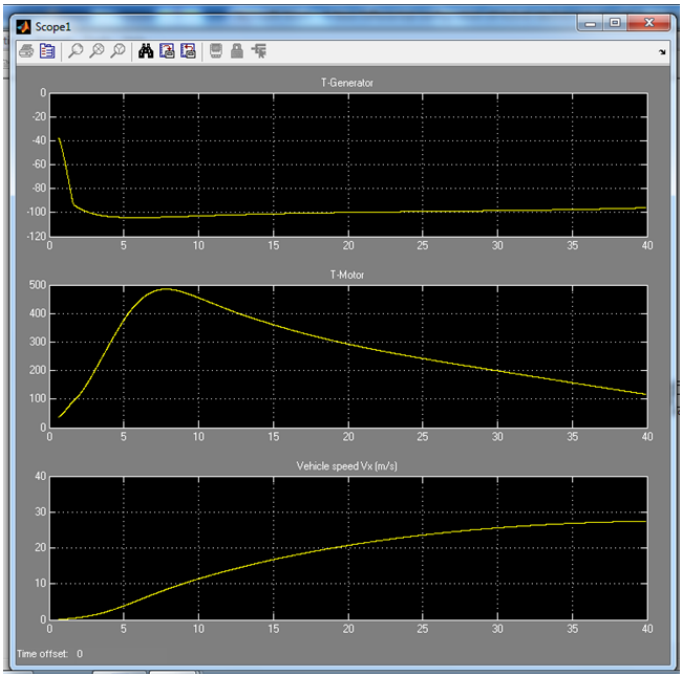

Figure (7). Simulation graphs of generator torque, motor torque and vehicle speed.

performance. Driving an IC engine within its reference torque through the use of torque loop is a new control strategy developed by many researchers [7].

7. Conclusions

The electrical torque gain (γ) which is the ratio of motor torque to the generator torque is drawn in Figure (8) against the relative velocity of the vehicle . The relative velocity of the vehicle at any time is the division of the current velocity (V_x) by the top gear velocity (V_T). From Figure (8) it is clear that the electrical torque gain γ is acting as a five-speed gear box with automatic shifting .As the relative speed reaches 1 the ratio approximates 1 . This means that the differential configuration acts together with the torque loop as a virtual (CVT).
Many researchers proved the validity of their new model by showing its robustness against load uncertainties[6]. Here , the new developed model is subjected to a step load.
Figure (9) shows the shift down capabilities of the

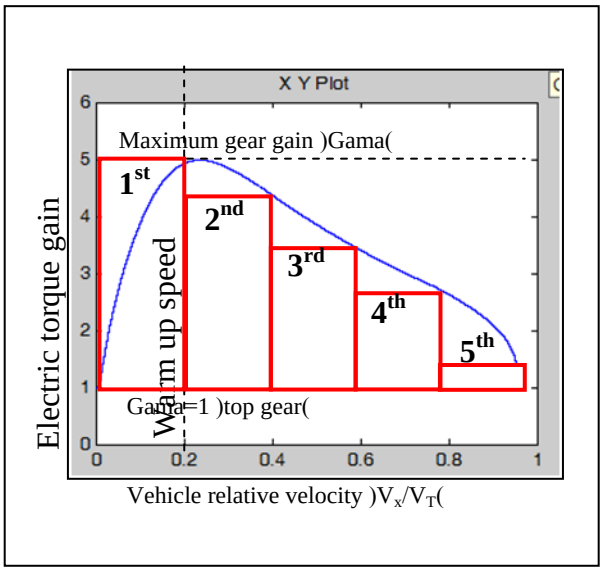

Figure (8). Gama verses relative speed.

current virtual Gear box .The Vehicle is subjected to a step force of 2000N at (T=10 sec and for 5 sec period).

During the first 10 seconds the torque gain starts to shift down automatically until it reaches about 3.2 at T=10sec . At this moment the step load is applied against the vehicle . The Value of Gama starts to increase again (this mean a shift down gear in a mechanical gear box).It is exactly the desired behaviour of standard automatic gear box . It automatically shifts down when load is increased and automatically shifts up when load decreases .

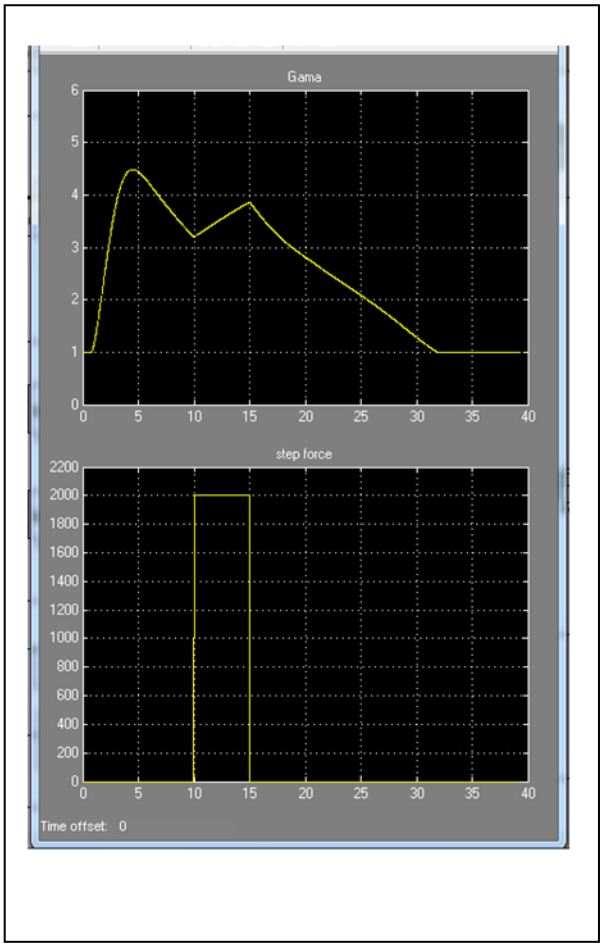

Figure (9). Robustness against step load.

8. References

[1] Chau, K .T and Wong Y.S, "Ovserview of power management in hybrid electric vehicles " , Journal of Energy Conversion and Management , Vol .43,pp 1953–1968,2002

[2] Bayindir, K .C., Gzüküçük,M .A .and AhmetTeke, "A comprehensive overview of hybrid electric vehicle :Powertrain configurations, powertrain control techniques and electronic control units" , Journal of Energy Conversion and Management, Vol.52 ,pp1305-1313,2011.

[3] Cajander, D .and Le-Huy, H .," Design and optimization of a torque controller for a switched reluctance motor drive for electric vehicles by simulation " , Journal of Mathematics and Computers in Simulation Vol .71 pp 333–344,2006

[4] Shigley, J .E., "Mechanical Engineering Design ", fifth edition, McGraw-Hill, 1989.

[5] Mehta,R. and Mehta V.K., "Principles of Electrical Machine", S Chand & Co Limited,2011.

[6] Ahmed N .Abdalla, ZulkarnainLubis, Mortaza bin Mohamed, Zalini Mohammad Ali and MohamadAzlan Mat Hussin, "A new series-parallel hybrid electric vehicle configuration based on an induction motor coupled to a DC machine ", Journal of Scientific Research and Essays Vol .5 (24), pp .4034-4043, 18 December, 2010.

[7] Ali, A .K ., kheioon, E .A .and Ali M .K ."A New anticipatory speed-controller for IC engines based on torque sensing loop " , Iraq J.of Electrical and Electronic Engineering, Vol.6 No.1, pp 16-21 ,2010.

Theoretical and Experimental Analysis of Flat Plate Collector

Raed Sabri Hameed

Technical College – Basrah

Abstract

In this work a flat plate collector was designed and manufactured with dimension of (100cm×160cm×20cm) and analyzed experimentally and theoretically. The designed FPC consist of Nine pipes with (2.223cm in diameter with 140cm long) welded above the plate to act as heat removal fluid passage ways. The flow inside the pipes can takes place by forced convection. However, certain energy absorbed by the plate is lost to atmosphere due to higher temperature of the plate. Effect of plate temperature on efficiency and top loss coefficient studied for different wind velocities and different air temperature. Effect of emissivity of absorber plate on top loss coefficient was estimated.

The obtained result showed that the efficiency of FPC increase by 3% with the increase in ambient temperature by 8˚C, the efficiency decrease with the increase in plate temperature and the top loss coefficient increase when the emissivity of absorber plate increase and when wind velocity increase. The comparison of result showed a good agreement.

المستخلص

في هذا العمل تم تصميم وبناء مجمع شمسي نوع الوسادة بابعاد (100cm×160cm×20cm) وتم تحليل المنظومة عمليا و نظريا. المجمع الشمسي يتكون من تسع انابيب تمتلك قطر 2.223cm وطول 140cm تكون هذه الانابيب ملحومة على صفيحة لتقوم بتحويل الحرارة الممتصة الى المائع الذي يجري في الانابيب. ان جريان المائع في الانابيب يكون من خلال الحمل القسري. قسم من الحرارة الممتصة سوف تنتقل الى المحيط بسبب ارتفاع درجة حرارة الصفيحة و الانابيب. تم دراسة تاثير درجة حرارة صفيحة الامتصاص على كفاءة المنظومة وعلى معامل فقدان الحرارة العلوي وتم دراسة تاثير انبعاثية صفيحة الامتصاص كذلك.

بينت النتائج التي تم الحصول عليها ان كفاءة المجمع الشمسي تزداد بمقدار 3% بزيادة درجة حرارة الهواء بمقدار 8 ْم وتنخفض الكفاءة مع زيادة درجة حرارة صفيحة الامتصاص ويزداد معامل فقدان الحرارة العلوي مع زيادة انبعاثية صفيحة الامتصاص ومع زيادة سرعة الرياح.

مقارنة النتائج اظهرت تقارب جيد.

1. Introduction

Solar power is the result of converting sunlight into heat. Sunlight can be converted directly to heat using Flat–Plate Collectors. The flat plate collectors are based on two important principles: a black base that absorbs the solar radiation better than any other color and a glass lid that is needed to keep the heat in. A typical flat–plate solar collector is shown in Figure (1). When solar radiation passes through a transparent cover and impinges on the blackened absorber surface of high absorptivity, a large portion of this energy is absorbed by the plate and transferred to the transport medium in the fluid tube carried a way for storage or use. The underside of the absorber plate and the two sides are wall insulated to reduce conduction losses. The liquid tubes can be welded to the absorbing plate or they can be an integral part of the plate. The liquid tubes are connected at both ends by large diameter header tubes. The header and riser collector are the typical design for flat–plate collectors.

When a certain amount of solar radiation falls on the surface of a collector, most of it is absorbed and delivered to the transport fluid, and it is carried away as useful energy. However, as in all thermal systems, heat losses to the environment by various modes of heat transfer are inevitable. The thermal network for a single-cover, flat-plate collector in terms of conduction, convection, and radiation is shown in Figure (2-a) and in terms of the resistance between plates in Figure (2-b).

The advantages of flat–plate collectors are that they are inexpensive to manufacture they collect both beam and diffuse radiation and they are permanently fixed in position so no tracking of the sun is required.

In 2005 Christoph trink l and et l ,[1] Studied the performance of flat plate and evacuated tube collectors and they found that both collectors are considered to be suitable for solar heating in Central European Climates. The vacuum tube collector, however, does not reach the additional energy yield expected.

In 2006, O.A. Ogunwole [2] presented a mathematical model and experimental test for Flat Plate Collector Solar Cooker and found that the temperature to which the cooker could be raised depended on the solar energy intensity and the period of sunshine.

In 2008, Fabio Struckmann . [3] developed a mathematical model to simulate the performance of flat plate collector. The most important measure is the collector efficiency. A more precise and detailed analysis should include the fact, that the overall heat loss coefficient and other factors as the heat removal factor are not constant values.

In 2009 Y. Raja Sekhar and etl., [4] analyze theoretically and experimentally a flat plate collector with a single glass cover. They conclude that the emissivity of the absorber plate has a significant impact on the top loss coefficient and consequently on the efficiency of the Flat plate collector.

The objective of the present work is to evaluate the heat loss coefficients and calculate the efficiency of designed flat plate collector for AL-Basra city in Iraq.

2. Experimental setup

The schematic of the experimental setup is shown in Figure (3). One sheet of Glass used with 7mm thickness to cover solar collector above a plate of iron (80cm×146cm) coated with black to maximize the energy collection. Nine pipes (2.223cm in diameter with 140 cm long) welded above the plate to act as heat removal fluid passage ways. A water tank of iron with (17cm×17cm×70cm) used as storage tank. In order to minimize the heat loss from the back and side of the collector the insulation of wall with 3.81cm thickness was used. The case of aluminum used surrounds the aforementioned components and protects them from dust, moisture, and any after material. To measure the temperature of water at inlet and outlet, two thermocouples located inside the pipes as shown in Figure (3). One of the thermocouples is placed on the center of plate to measure the plate temperature.

3. Analysis

Assuming one-dimensional heat flow, under steady state conditions. In a steady state, the rate of useful energy collected from a collector of area A_c can be obtained from [5]:

$$Q_u = \dot{m}\, c_p\, (T_o - Ti) \quad (1)$$

The thermal energy lost from the collector to the surroundings by conduction, convection, and infrared radiation is represented by:

$$Q_l = U_L\, A_c\, (T_P - T_a) \quad (2)$$

Where: U_L: The overall heat loss coefficient

The overall heat loss coefficient is a complicated function of the collector construction and its operating conditions, given by the following expression [5]:

$$U_L = U_t + U_b + U_e \quad (3)$$

The overall top heat loss coefficient is a function of various parameters which include the temperature of the absorber plate, glass cover and ambient, emissivity of absorber and glass

cover, spacing between the absorber and glass cover L, tilt angle of the collector β, number of glass covers, etc given by[4]:

$$U_t = \frac{1}{\frac{N_g}{\frac{C}{T_P}\left[\frac{T_P - T_a}{N_g + f}\right]^{0.33}} + \frac{1}{h_w}} + \frac{\sigma\left(T_P^2 + T_a^2\right)(T_P + T_a)}{\frac{1}{\epsilon_P + 0.05 N_g (1-\epsilon_P)} + \frac{2N_g + f - 1}{\epsilon_g} - N_g} \quad (4)$$

$$f = (1 - 0.04h_w + 0.0005h_w^2)\left(1 + 0.091N_g\right)$$

$$C = 365.9(1 - 0.00883\beta + 0.0001298\beta^2)$$

$$h_w = \frac{8.6V^{0.6}}{L^{0.4}}$$

The energy loss from the bottom of the collector is first conducted through the insulation and then by a combined convection and infrared radiation transfer to the surrounding ambient air; because the temperature of the bottom part of the casing is low the radiation term can be neglected thus the energy loss is given by:

$$U_b = \frac{1}{\frac{t_b}{k_b} + \frac{t_c}{k_c} + \frac{1}{h_{c,b-a}}} \quad (5)$$

In a similar way the heat transfer coefficient for the heat loss from the collector edges can be obtained from:

$$U_e = \frac{1}{\frac{t_e}{k_e} + \frac{t_c}{k_c} + \frac{1}{h_{c,e-a}}}$$

Efficiency of FPC can be calculated from:

$$\eta = \frac{Q_u}{Q_u + Q_l}$$

4. Results and discussions

Comparison of efficiency of designed FPC with that obtained by [4] shows in Figure (5). The effect of ambient temperature on the efficiency of the FPC is shown in Figure (6). The efficiency is increase with the increase in ambient temperature due to reduction in heat loss from the system and the efficiency is decrease with the increase of absorber plate temperature due to the increase of losses from absorber plate. The effect of wind velocity on top loss coefficient is shown in Figure (7). As the wind velocity increase the top loss coefficient increase due to increasing in amount of heat rejected to atmosphere. The variation of top loss coefficient with absorber plate temperature is shown in Figure (8). As the emissivity of absorber plate increases the top loss coefficient increases.

From the obtained result it can be included that the efficiency of FPC increase by 3% with the increase in ambient temperature by 8° C, the efficiency of FPC decrease with the increase in absorber plate temperature and the top loss coefficient increase when the emissivity of absorber plate increase and when wind velocity increase.

5. Conclusion and recommendation

The experimental and theoretical analysis of FPC has been described. The efficiency of FPC collector increase with the increase in ambient temperature and decrease with the increase in absorber plate temperature. The top loss coefficient increase when the emissivity of absorber plate increase and when wind velocity increase.

The future work may be include study the effect of collector tilt angle, number of glass cover and use glass solar concentrator on efficiency of FPC.

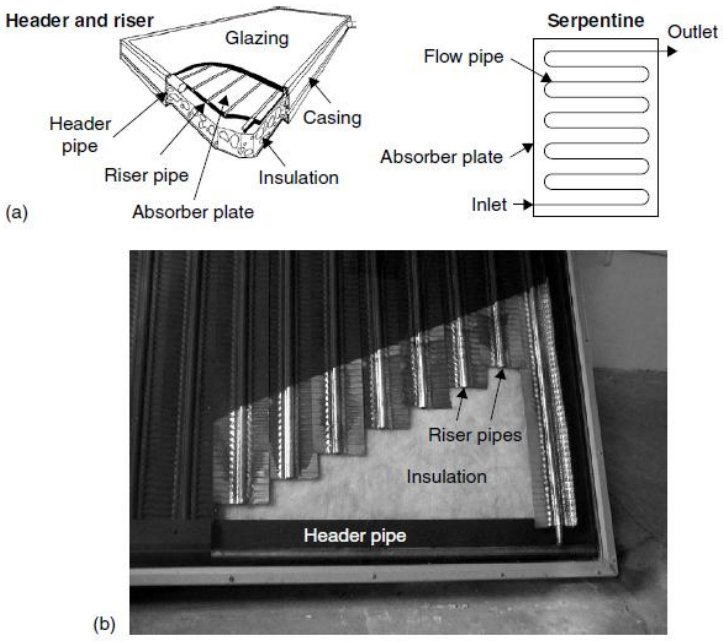

Figure (1) . Typical flat-plate collector. (a) Pictorial view of a flat-plate collector. (b) Photograph of a cut header and riser flat-plate collector.[5]

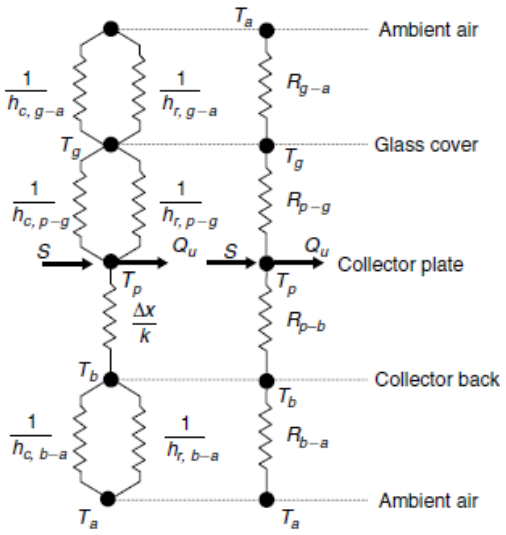

Figure (2). The thermal network for a single-cover, flat-plate collector. (a)In terms of conduction, convection, and radiation (b)In terms of the resistance between plates.

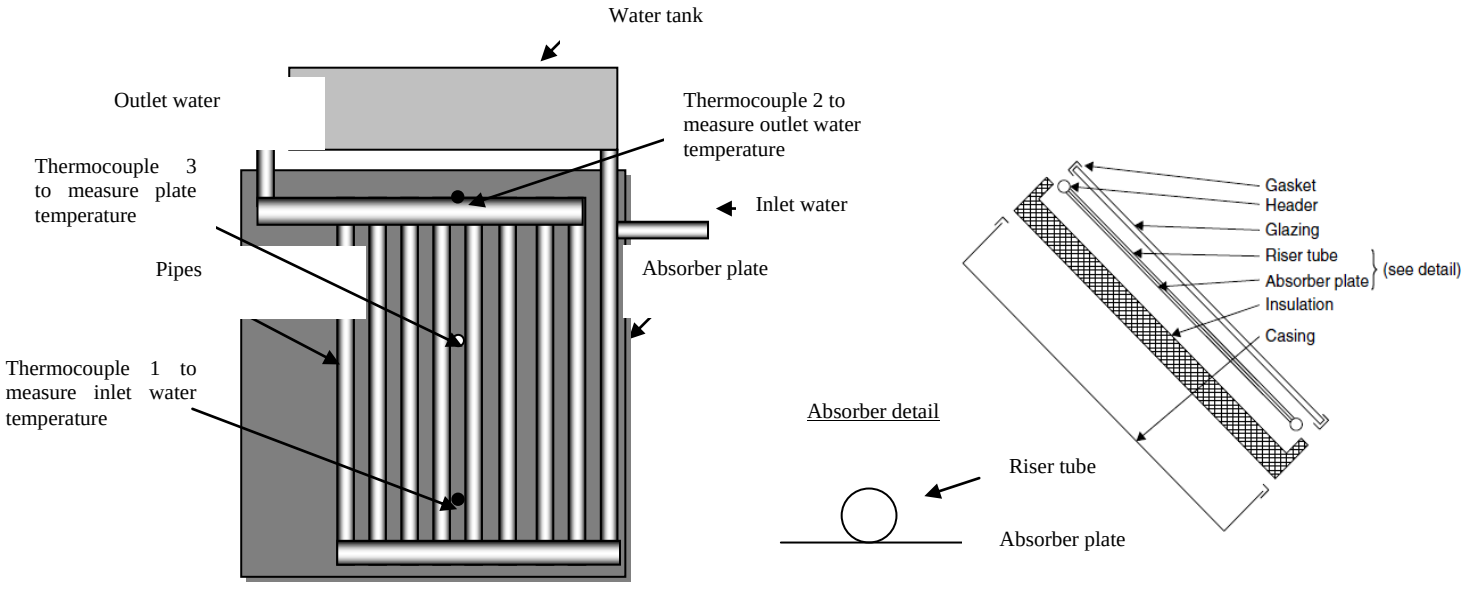

a) Front view of flat plate collector

b) exploded view of flat plate collector and absorber details.

Figure (3). Schematic diagram for flat plate collector.

Figure(4). Different photograph view for the Manufactured Flat-Plate Collector.

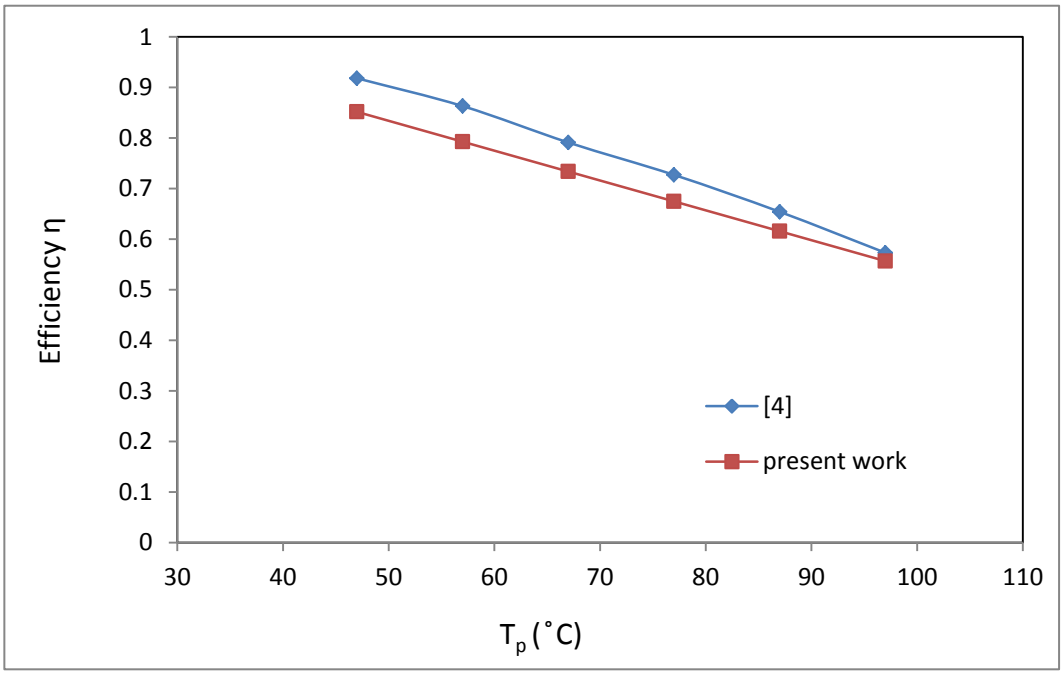

Figure (5) . Comparison of efficiency obtained by [4] with present work.

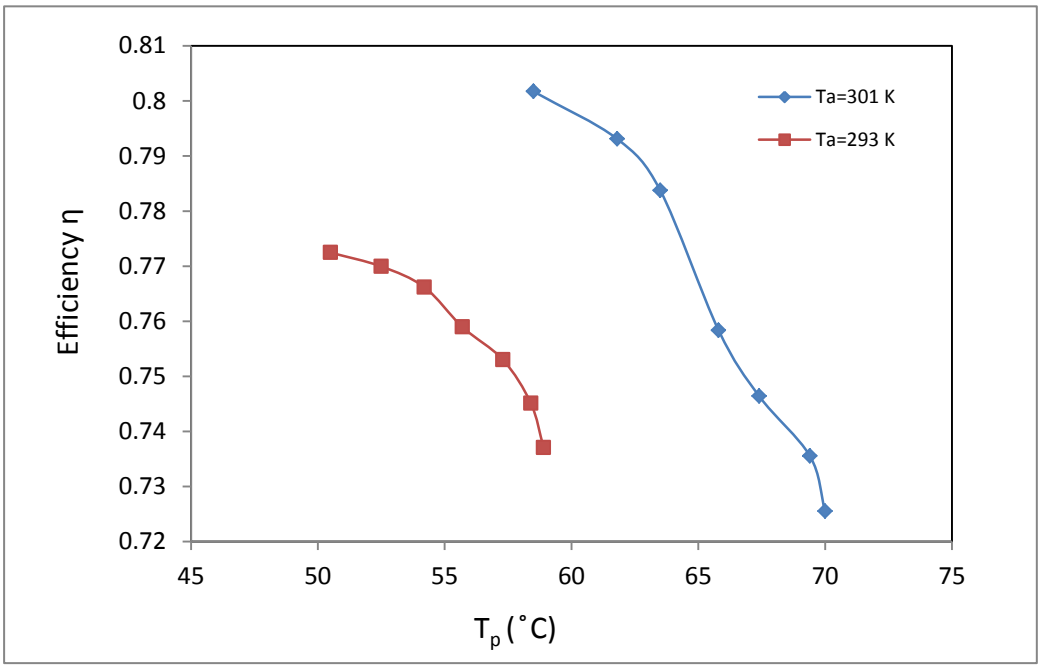

Figure (6) . Effect of absorber plate temperature on efficiency of FPC for two different ambient temperature.

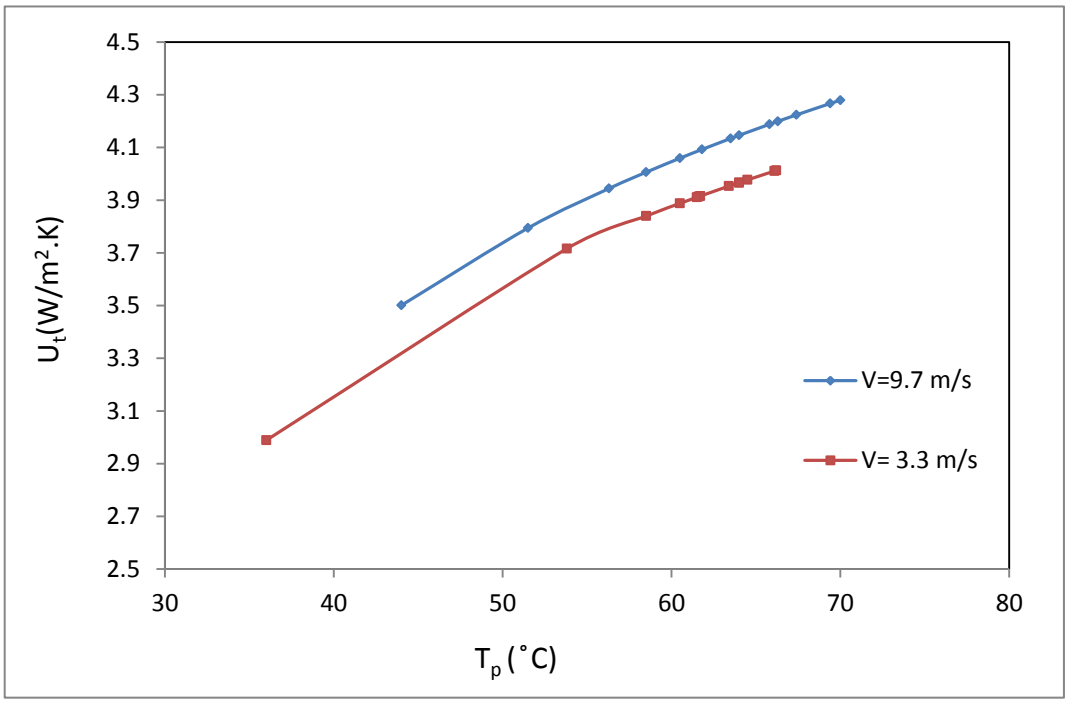

Figure (7). Effect of absorber plate temperature on top loss coefficient for different wind velocity.

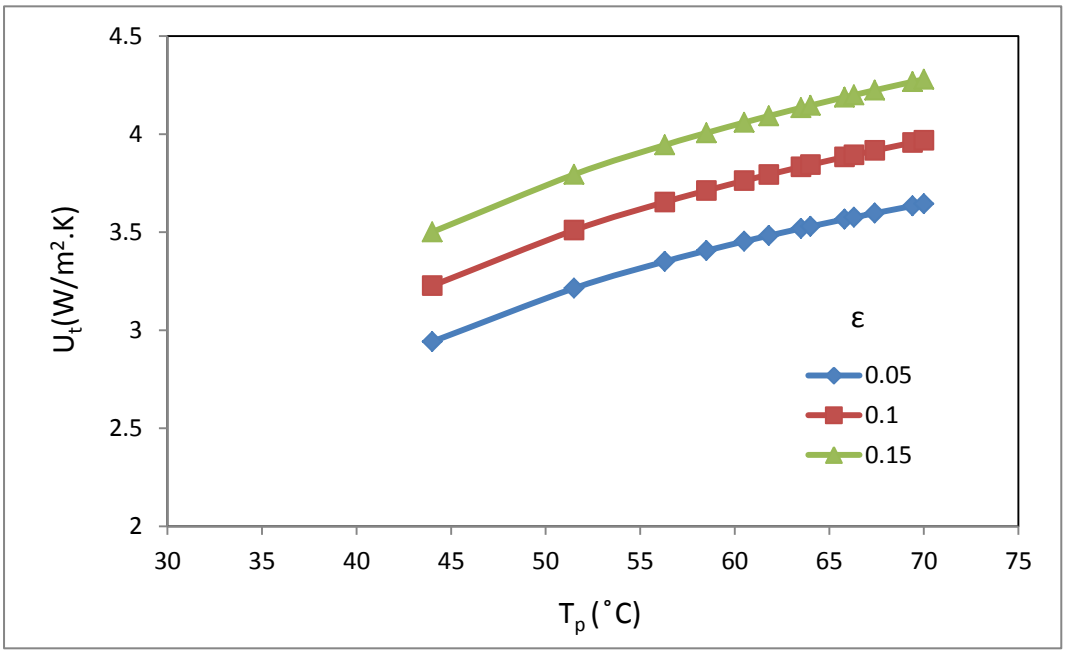

Figure (8). Effect of absorber plate temperature on top loss coefficient for different value of (ϵ_p).

6. References

[1] Christoph Trinkl and etl., "Performance of Vacuum Tube and Flat Plate Collectors Concerning Domestic Hot Water Preparation and Room Heating", 2nd European Solar Thermal Energy Conference, 2005.

[2] O.A. Ogunwole, " Flat Plate Collector Solar Cooker ", Department of Mechanical Engineering, Federal University of Technology, Nigeria 2006.

[3] Fabio Struokmann, "Analysis of a Flat-plate Solar Collector ", Dept. of Energy Science, Faculty of Engineering, Lund University, Project Report, Sweden, 2008.

[4] Y. Raja Sekhar, K. V. Sharma and M. Basaveswara Rao, "Evaluation of Heat Loss Coefficients in Splar Flat Plate Collectors", ARPN Journal of Engineering and Applied Sciences, Vol. 4, No. 5, JULY 2009.

[5] Soteris Kalogirou, "Solar Energy Engineering: Processes and Systems", Elsevier's Science & Technology, United States of America, 2009.

7. Nomenclature

A Area, m^2

h convection heat transfer coefficient, W m^{-2} K^{-1}

h_w wind loss coefficient, W m^{-2} K^{-1}

k conductivity W m^{-1} K^{-1}

N number of glass cover

L length of absorber pipes, m

Q Energy, W

T Temperature, ℃

t Thickness, m

U_l Overall loss coefficient, W m^{-2} K^{-1}

U_t Overall top loss coefficient, W m^{-2} K^{-1}

U_b Overall loss coefficient for the heat loss from back to ambient, W m^{-2} K^{-1}

U_e Overall loss coefficient for the heat loss from edge to ambient, W m^{-2} K^{-1}

Greek symbols

ε Emissivity

σ Stefan-Boltzman constant, W m^{-2} K^{-4}

β Collector tilt angle

Sub scripts

a ambient

b back

c collector

e edge

p absorber plate

g glass cover

u useful

l lost

o out

i in

Real-time Alert of Motion Detection Using Microcontroller

Haithm Abdul Raheem Taha

Al-Mostanserya University

Elect. Eng. Dept.

College of Engineering

Abstract

This paper addresses the problem of motion detection and moving objects of variable appearance in challenging scenes rich with features and texture. It is made particularly difficult by the nature of objects encountered in such scenes. The research included a method which uses fast motion detection and segmentation as constraint of differences between frames of video, and when changes in each pixel of an image, will alert start and message displayed on LCD that plugged to microcontroller.

Keywords: Motion Detection; Microcontroller; LCD; Alarm; Interface.

المستخلص

الغرض من البحث هو التنبيه إثناء عملية الكشف عن الحركة وإثناء تحريك الأجسام الموجودة في المشهد الذي يحتوي على الكثير من التفاصيل والأجسام الأخرى. والعمل المقترح هو باستخدام طريقة سريعة للكشف عن الحركة وذلك بالفرق بين الصور المصورة عبر التصوير الفيديوي، وعندما يكون التغيير في اي عنصر من عناصر الصورة (البكسل)، يتم التنبيه بإرسال رسالة إلى دائرة تحتوي على معالج دقيق وشاشة عرض صغيرة لعرض الرسالة التنبيهيه وتشغيل منبه صوتي إثناء عملية الكشف عن الحركة.

1. Introduction

A video sequence is a much richer source of visual information than a still image. This is primarily due to the capture of motion; while single image provides a snapshot of a scene, a sequence of images registers the dynamics in it. The registered motion is very strong cue for human vision; that can easily recognize objects as soon as they move even if they are inconspicuous when still. In this paper, an application designed require image points be identified as moving or not, or that it be measured how they move. The first task is referred to as motion detection, whereas the latter is referred to alert using microcontroller which considered so important task in security especially in government offices and special sectors that need kind of security systems found in place and do work which considered difficult for human to do, and here come the benefit of automation devices self-controlled[1].

2. Study of proposed work

The objective of this work was to develop a surveillance system which would detect motion in a live video feed and if motion is detected, then to activate a warning system and display warning message on LCD.

The activation of an alarm would help in nullifying a threat of security. The proposed system is shown in the Figure (1).

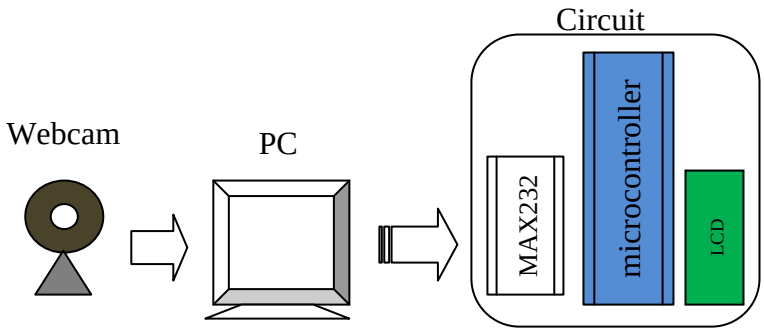

Figure (1). System proposed of motion detection.

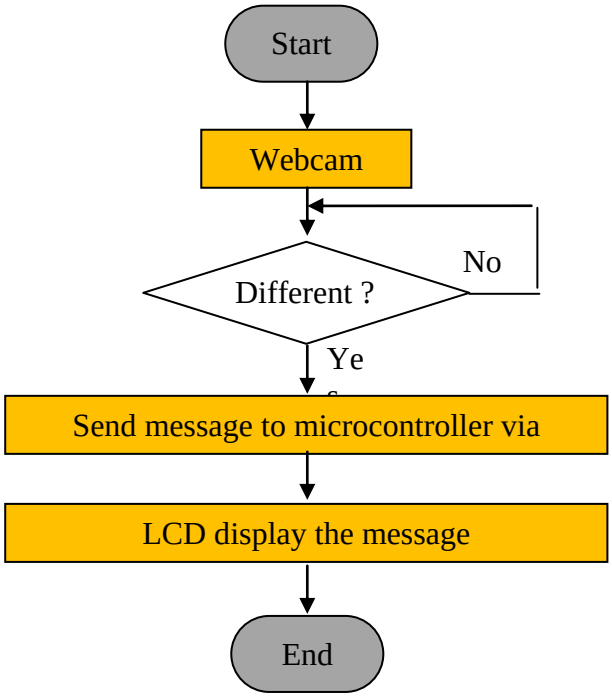

Figure (2). Flow chart of proposed work.

3. Motion detection

Motion detection is, arguably, the simplest of the motion related tasks, i.e., detection, estimation, and segmentation. Its goal, is to identify which image points, or more generally which regions, of the image have moved between two time instants. As such, motion

detection applies only to images acquired with a static camera. However, if camera motion can be counteracted, by global motion estimation and compensation, then the method equally applies to images acquired with a moving camera[2].

It is essential to realize that the motion of image points is not perceived directly but rather through intensity changes. However, such intensity changes over time may be also induced by camera noise or illumination changes. Moreover, object motion itself may induce small intensity variation or even none at all[2].

4. Image differencing for change detection

Often it is of interest to detect changes that occur in images taken of the same scene but at different times. If the time instants are closely placed, e.g., adjacent frames in a video sequence, then the goal of change detection amounts to image motion detection. There are many applications of motion detection and analysis. Detected motion is also useful for tracking targets and for recognizing objects by their motion[3].

If the time separation between frames is not small, then change detection involves the discovery of gross scene changes. This can be used for security or surveillance cameras, or in automated visual inspection systems. Suppose that f_1 and f_2 are images to be compared.

$$g = |f_1 - f_2| \quad (1)$$

The absolute difference image will embody those changes or differences that have occurred between the images. At coordinates *n* where there has been little change, g(n) will be small. Where change has occurred, g(n) can be quite large. Figure (3) depicts image differencing. In the difference image, large changes are displayed as points appear over the place of change in the image. Since significant change has occurred, there are many pointed intensity. This difference image could be processed by an automatic change detection algorithm. A Simple series of steps that might be taken would be to binaries the difference image, thus separating change from nonchange, counting the number of high change pixels, and finally, deciding whether the change is significant enough to take some action. Sophisticated variations of this theme are currently in practical use[3].

(a) Original placing scene; **(b) motion detect with pointing non-matched area.**

Figure (3). Image differencing example.

Both continuous and discrete representations of motion and images will be used, with bold characters denoting vectors. May be $x=(x_1,y_1)^t$ be a spatial position of a pixel in continuous coordinates may be expression as $x \in R2$ within image limits, and let I_t denotes image intensity at time *t*. Then, $I_t(x) \in R$ is limited by dynamic range of the sensing device (webcam in our study). Before images can be manipulated digitally, they have to be sampled and quantized. Let $n=(n_1,n_2)^t$ be a discretized spatial position in the image that corresponds to *x*. Similarly, let *k* be a discretized position in time, also denoted t_k. It is assumed here that images are either continuous or discrete simultaneously in position in amplitude. Consequently, the same symbol *I* will be used for continuous and quantized intensities; the nature of *I* can be inferred from its argument (continuous valued for *x* and quantized for (*n*)[4].

Motion in continuous images can be described by a velocity vector $v=(v_1,v_2)T$. Whereas $v(x)$ is a velocity at spatial position x,v_t will denote a velocity field or motion field, i.e., the set of all velocity vectors within the image, at time *t*. Often the computation of this dense representation is replaced by the computation of a small number of motion parameters b_t with the benefit of reduced computational complexity. The, v_t is approximated by b_t by means of a known transformation. For discrete images, the notion of velocity is replaced by displacement (*d*) [4].

5. Hypothesis testing with adaptive threshold

The motion detection methods presented thus far were based solely on image intensities and made no a priori assumptions about the nature of moving areas. however,

moving object usually creates compact, closed boundaries in the image plane, i.e., if an image point is declared moving[5], it is likely that its neighbor is moving as well (unless the point is on a boundary) and the boundary is smooth rather than rough. To take advantage of this a priori information, hypothesis testing can be combined with Markov random field models.

Let E_k be a Markov Random Field (MRF) of all labels assigned at time t_k, and let e_k be its realization. Let us assume for the time being that $e_k(n)$ is known for all n except I. Since the estimation process is iterative, this assumption is not unreasonable; previous estimates are known at $n \neq I$. Thus, the estimation process is reduced to a decision between $e_k(I)=M$ and $e_k(I)=S$. Let the label field resulting from $e_k(I)=M$ be denoted by e_k^M and that produced by $e_k(I)=S$ be e_k^S. Then, the decision rule for $e_k(I)$ can be written as follows[3]:

$$\frac{P(\rho_k|e_k^M)}{P(\rho_k|e_k^S)} \underset{S}{\overset{M}{\lessgtr}} \theta \frac{P(E_k = e_k^S)}{P(E_k = e_k^M)} \tag{2}$$

where P is a probability distribution governing the MRF E_k. By making the simplifying assumption that the temporal differences $\rho_k\ (n)$ are conditionally independent, i.e., $P(\rho_k|e_k) = \prod_n P(\rho_k(n)|e_k(n))$, then further rewrite eq.(2) as[3]

$$\frac{P(\rho_k(I)H_M)}{P(\rho_k(I)H_S)} \underset{S}{\overset{M}{\lessgtr}} \theta \frac{P(E_k = e_k^S)}{P(E_k = e_k^M)} \tag{3}$$

The hypothesis H_M means that $e_k(I)=M$ and H_S means that $e_k(I)=S$. All constituent probability densities from the left-hand side of Eq.(3), except at I, cancel out since $e_k M$ and $e_k S$ differ reasonable in stationary areas (temporal differences are mostly due to camera noise), it is less so in the moving areas. However, a convincing argument based on experimental results can be made in favor of such independence.

To increase the detection robustness to noise, the temporal differences should be pooled together, for example within a spatial window W_1 centered at I. This leads to the evaluation of the likelihood for all ρ_k within W_1 given the hypothesis H_M or H_S at I. Under the assumption of zero-mean Gaussian density P with variances σ_M^2 and σ_S^2 for H_M and H_S, respectively, and assuming that $\sigma_M^2 \gg \sigma_S^2$ the final hypothesis becomes[3]:

$$\sum_{n \in W_1} \rho_k^2(n) \underset{S}{\overset{M}{\gtrless}} 2\sigma_S^2 \left(-ln\theta + N \ln \frac{\sigma_M}{\sigma_S} + \ln \frac{P\ (E_k = e_k^S)}{P\ (E_k = e_k^M)} \right) \tag{4}$$

where N is the number of pixels in W_1. In case the a priori probabilities are identical or fixed (independent of the realization e_k), the overall threshold depends only on model variances. Then, for increasing σ_S^2, the overall threshold rises as well, thus discouraging M labels (as camera noise increases only large temporal differences should induce moving

labels). Conversely, for decreasing σ_S^2, the threshold falls, thus biasing the decision toward moving labels. In the limit, as $\sigma_S^2 \rightarrow 0$ the threshold becomes 0; for a noiseless camera even the slightest temporal difference will induce a moving label[1].

By suitably defining the a priori probabilities one can adapt the threshold in response to the properties of e_k. Since the required properties are object compactness and smoothness of its boundaries, a simple MRF model supported on a first-order neighborhood with two-element cliques C{n,I} and the following potential function[3]

$$V_{nl} = \begin{cases} 0 & if \;\; e_k(n) = e_k(I) \\ \beta & if \;\; e_k(n) \neq e_k(I) \end{cases} \tag{5}$$

The eq.(5) is appropriate. Whenever a neighbor of n has a different label than $e_k(n)$, a penalty $\beta > 0$ is incurred; summed over the whole field it is proportional to the length of the moving mask boundary.

$$p(E_k = e_k) = \frac{1}{Z}\exp\left(-\frac{1}{T}\sum_{\{n,I\}} V_{nl}\right) \tag{6}$$

Thus, the resulting probability will increase for configurations with smooth boundaries and will reduce for those with rough boundaries. More advanced models, for example, based on second-order neighborhood systems with diagonal cliques, can be used similarly[3].

6. Interfacing and microcontroller

Figure (4) illustrates , the schematic of the controller that receives a message from software of motion detection. This design uses a microcontroller 8051 family (AT89S52) with LCD (16*2) to display the message that is sent via RS232 port to microcontroller[6].

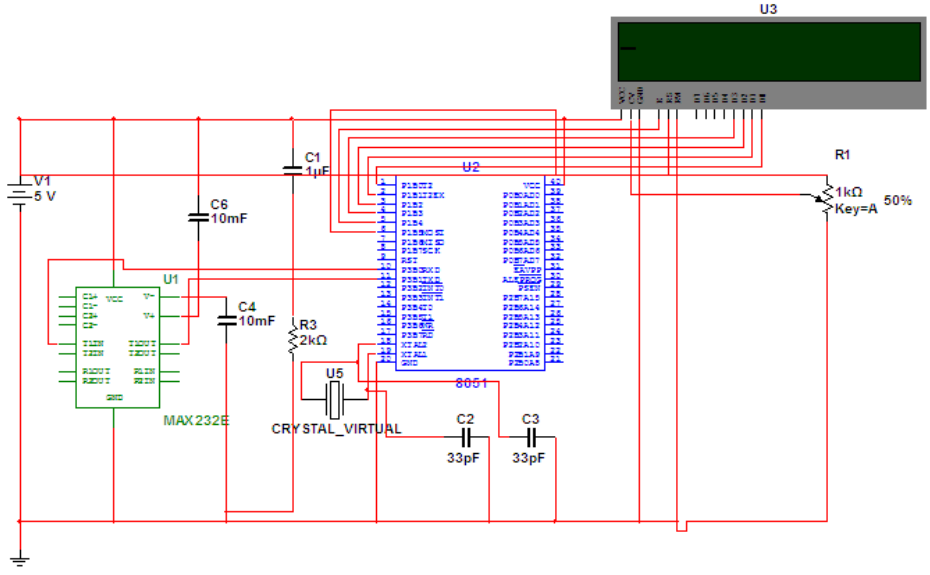

Figure (4). Schematic of the proposed work.

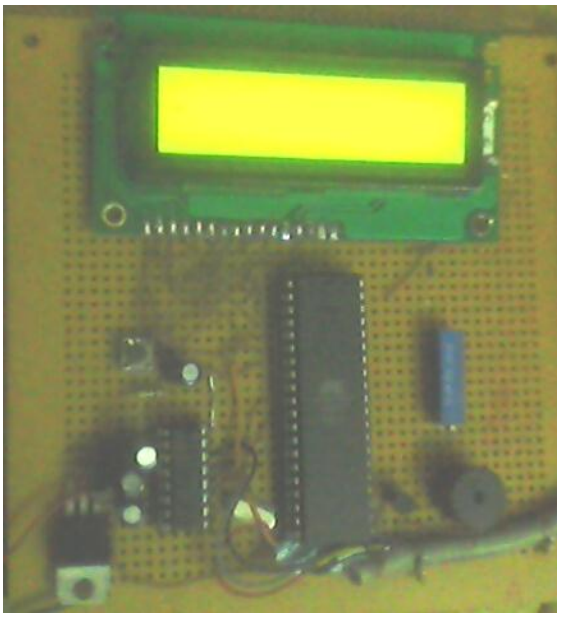

Figure (5). Practiced design circuit of proposed work.

7. Results

A webcam starts after specify the port number of the RS232, which allowed later control via this port. No actions will take while there is no motion happened in front of the webcam that can pass the differences part and send a message. When motion detected then a statement used to send a message to microcontroller via Rs232 port, is descript below:

Mscomm1.Output = "Motion Detected"

As shown in Figure (6), shows when a microcontroller start or when restart.

Figure (6). Starting/Restarting a microcontroller.

Below the snapshots take when an motion detected. As noted in Figure (7) the points of green color drawn around the object or any differences happening in an image.

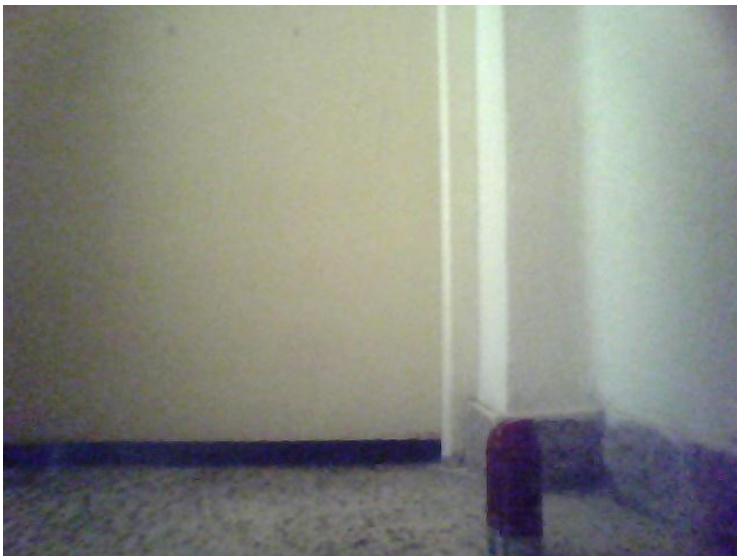

Figure (7). Snapshot of object when no motion detected.

Figure (8). Snapshot of object when motion detected.

Figure (9). Snapshot of object when no motion detected.

Figure (10). Snapshot of object when motion detected.

And when a motion/movement detected, microcontroller start display that a movement detect, and the alarm will start after 10 seconds as shown in Figure (11).

Figure (11). Movement detection display.

After detection happened and microcontroller start a notification for the movement found, an alarm will started, as shown in Figure (12).

Figure (12). Alarm started display.

8. Conclusion

In this paper, camera motion detection methods using a differences of images generated by the video (webcam) are described. The proposed method is evaluated by using a circuit implemented a microcontroller and LCD (16*2) to enhance the security of sensitive

places and sectors need to watch automatically from any kind of movement of objects or get through inside the scene that observed.

The advantage of proposed system is good solution for victim detection motion detection and good visibility during daytime and relatively low initial cost, low power, built-in electronic package, small size, and ease of interface with its digital output. And the disadvantage can fail if the sensor mat is not placed on a hard board.

The proposed system has present an algorithm based on MRF modeling for motion detection in image sequences, spatial and temporal interactions between pixels are modeled by MRF. This system communicates with a modem or PC to electronic design circuit sending and receiving data, and then direct the program to understand its operation. And the operation here is based on image processing where image been changed or any part of the image, and then calculation between two images (the original and last image). PC's serial data acquisition interfaces require the sending and receiving of data to operate. To communicate with the serial port using Visual Basic, the MsComm control must be utilized to allow serial data transfer via a serial port (Com1-Com4).

When detection of motion happens, the signal send to microcontroller which interfaced to same system has been detect a motion. A microcontroller received this data via MAX232 which convert the data of serial to TTL/CMOS, when receive a data, the microcontroller will find out what kind of data, is there a detection or not, if there is are a motion detection happened, then will send a message to serial LCD to be displayed, and in same time will set the alert on for 5 seconds.

9. Reference

[1] Al Bovik; 2002; "Handbook of Image and Video processing"; Elsevier Academic Press.

[2] Anthony C. Caputo; 2010; "Digital Video Surveillance and Security"; Butterworth-Heinemann Press.

[3] Janusz Konard; 2002; "Motion Detection and Estimation"; Elsevier Academic Press.

[4] Masaki Naito, Kazunori Matsumoto; 2006; "Camera Motion Detection Using Video Mosaicing"; Multimedia and Expo, IEEE International Conference.

[5] Jonathan Glumac; 2009;"Motion Detection and Object Tracking with Interactive Surfaces"; Redfish Group, Worcester Polytechnic Institute (WPI).

[6] Chris Braithwaite, Fred Cowan, Hassan Parchizadeh; 2004; "8051 Microcontroller, An Applications Based Introduction"; Elsevier Academic Press.